https://doi.org/10.5194/acp-2020-587
Preprint. Discussion started: 5 August 2020

Atmospheric Chemistry and Physics Discussions

Comparison of Chemical Lateral Boundary Conditions for Air Quality Predictions over the Contiguous United States during Intrusion Events

Youhua Tang[1,2], Huisheng Bian[3,4], Zhining Tao[3,5], Luke D. Oman[3], Daniel Tong[1,2,6], Pius Lee[1], Patrick C. Campbell[1,2], Barry Baker[1,2], Cheng-Hsuan Lu[7,10], Li Pan[8,9], Jun Wang[8], Jeffery McQueen[8], Ivanka Stajner[8]

1. NOAA Air Resources Laboratory, College Park, MD 20740, USA
2. Center for Spatial Information Science and Systems, George Mason University, Fairfax, VA
3. NASA Goddard Space Flight Center, Greenbelt, MD
4. University of Maryland at Baltimore County, Baltimore, MD
5. Universities Space Research Association, Columbia, MD 21046
6. University of Maryland, College Park, MD 20740, USA
7. Joint Center for Satellite Data Assimilation, Boulder, CO, USA
8. NOAA/NCEP/Environmental Modeling Center, College Park, MD, USA
9. I.M. Systems Group Inc., Rockville, MD
10. University at Albany, State University of New York, Albany, NY, USA

Abstract

The existing National Air Quality Forecast Capability (NAQFC) operated at NOAA provides operational forecast guidance for ozone and particle matter with aerodynamic diameter less than 2.5μm ($PM_{2.5}$) over the contiguous 48 U.S. states (CONUS) using the Community Multi-scale Air Quality (CMAQ) model. Currently NAQFC is using chemical lateral boundary conditions (CLBCs) from a monthly climatology, which cannot capture pollutant intrusion events originated outside of the model domain. In this study, we developed a model framework to introduce the time-varying chemical simulation from the Goddard Earth Observing System Model, version 5 (GEOS) as the CLBCs to drive NAQFC. The method of mapping GEOS chemical species to CMAQ CB05-Aero6 species was also developed. We then evaluated NAQFC's performance using the new CLBCs from GEOS. The utilization of the GEOS dynamic CLBCs showed an overall best score when comparing the NAQFC simulation with the surface observations during the Saharan dust intrusion and Canadian wildfire events in summer 2015: the PM2.5 correlation coefficient R was improved from 0.18 to 0.37 and the mean bias was narrowed from -6.74 $\mu g/m^3$ to -2.96 $\mu g/m^3$ over CONUS. The CLBCs' influences depended on not only the distance from the inflow boundary, but also species and their regional characteristics. For the PM2.5 prediction, the CLBC's effect on the correlations was mainly near the inflow boundary, and its impact on the background could reach farther inside the domain. The CLBCs also altered background ozone through the inflows of ozone itself and its precursors. It was further found that aerosol optical thickness (AOT) from VIIRS retrieval correlated well to the column CO and elemental carbon from GEOS, based on which the new CLBCs for wildfire intrusion event was derived. The AOT derived CLBCs successfully captured the wildfire intrusion events in our case study for summer 2018. It can be a useful alternative in case the CLBCs of GEOS are not available.

https://doi.org/10.5194/acp-2020-587
Preprint. Discussion started: 5 August 2020

Atmospheric Chemistry and Physics Discussions

1. Introduction

The chemical lateral boundary condition (CLBC) is one of the most important factors affecting the prediction accuracy of regional chemical transport models (Tang et al., 2009; Tang et al., 2007). It mainly plays two roles in the regional modeling system: 1) to impose the constraints with background concentrations and 2) to represent the external influence for intrusion events. The climatological static CLBCs can provide the first role for some long-lived pollutants, such as CO and O_3. Models like the Community Air Quality Multi-scale Model (CMAQ) hemispheric version (Mathur et al, 2017) can also get this constraint with its LBC along the equator. The second role of the CLBC, representing the influences of external intrusion events, can only be made with the dynamic (time-varying) CLBCs. Such CLBCs can only come from a global model, a regional model with bigger domain (Tang et al., 2007), or observed profiles (Tang et al., 2009).

As a regional chemical forecast system, the existing National Air Quality Forecast Capability (NAQFC) operated at NOAA needs proper CLBCs for its daily prediction. The current NAQFC uses the dust aerosol LBC from the NOAA Environmental Modeling System (NEMS) Global Forecast System (GFS) Aerosol Component (NGAC) (Lu et al, 2016; Wang et al, 2018), which is the GFS model coupled with Goddard Chemistry Aerosol Radiation and Transport (GOCART) aerosol mechanism (Chin et al., 2000, 2002; Colarco et al., 2010). Before the implementation of NGAC LBC, NAQFC used the background static profile LBC for aerosols described in Lee et al. (2017). For gaseous species, NAQFC uses the modified monthly averaged LBCs from the GEOS-Chem (Bey et al., 2001) simulation for year 2006 (Pan et al., 2014). To alleviate surface ozone over-predictions, the upper tropospheric ozone LBC from GEOS-Chem have been limited ≤ 100 ppbV.

The static gaseous LBC cannot capture the signals of some intrusion events, such as the biomass burning plumes from the outside of the domain, which could affect ozone and particle matter with aerodynamic diameter less than 2.5μm ($PM_{2.5}$). Tang et al. (2007) investigated the sensitivity of the regional chemical transport model (RCTM) to LBCs, and found that the background magnitude of the pollutant concentrations sometimes were more important than the variation of LBCs for the near-surface prediction over polluted areas, or the first role of the CLBC was more critical. Over the Contiguous United States (CONUS) domain, the prevailing inflow lateral boundary includes northern and western USA, where Canadian emission and long-rang transported Asian air-masses can affect the CONUS background. Southeastern States could encounter the Saharan dust intrusion during summer time, which usually resulted in a surface PM2.5 increase (Lu et al, 2016). In order to assess their impact, a proper CLBC from a global model that carries those signals is needed. In this study, we extracted the CLBC from the GEOS global chemical circulation model (GCCM) (Strode et al. 2019; Molod et al., 2012) in static (monthly average) and dynamic (3-hour varying) modes. The CMAQ runs with the GEOS CLBCs were then compared to the CMAQ base case and another run with the NGAC aerosol

https://doi.org/10.5194/acp-2020-587
Preprint. Discussion started: 5 August 2020


Atmospheric Chemistry and Physics Discussions

LBC for the summer 2015. During this period, the Canadian wild fire and Sahara dust affected the CONUS domain, which affected the Northern and Southern USA, respectively, and different CLBCs showed their impacts on the CMAQ regional predictions. In addition, we will investigate the method of using historical CLBCs with a certain indicator to derive a new CLBC for the future pollutant intrusion events in case an appropriate global CLBC is not available.

2. Model Configuration and Experiment Design

Current NAQFC is using CMAQ version 5.0.2, which includes CB05 gaseous chemical mechanism (Yarwood et al., 2005) with updated toluene (Whitten et al., 2010) and chlorine chemistry (Tanaka et al., 2003; Sarwar et al., 2007), and Aero6 (Sonntag et al., 2014) aerosol module driven by NOAA/NCEP's North American Mesoscale Model (NAM) forecasting. It has 12km horizontal resolution covering CONUS and 35 vertical layers up to 100 hPa. Anthropogenic and mobile emissions are the projected U.S. EPA National Emission Inventory (NEI) with base year 2011 and the point emissions have been updated with the U.S. EPA Continuous Emission Monitoring System (CEMS) for the target year (2015). Biogenic emissions are based on the Biogenic Emission Inventory System (BEIS) 3.14 (Pierce et al., 1998). Wildfire emission inside the CONUS domain is estimated using the U.S. Forest Service (USFS) BlueSky fire emissions estimation algorithm with the fire location information provided by NOAA Hazard Mapping System (HMS), which is satellite-based fire detection system with some manual analysis.

In this study, we conducted 5 model runs with different CLBCs (Table 1). The CMAQ base case uses the modified GEOS-CHEM 2006 monthly LBC (referred to as CMAQ_Base). The NGAC-LBC contains NGAC's GOCART aerosol dynamic LBC. The GEOS dynamic LBC (GEOS-LBC) is full chemistry for both gaseous and aerosol species. We also tested its corresponding monthly mean LBC (GLBC-monthly) for the temporal variation. Besides the normal global LBCs, an aerosol optical depth (AOT) derived Northern LBC (AOT-NLBC) is developed, which will be discussed later. These runs used the same settings except the CLBCs. The two CMAQ runs with dynamic CLBCs, the NGAC-LBC and GEOS-LBC, imported the corresponding LBC every 3 hours. The NGAC-LBC only updates the aerosol LBC from the NGAC global model and its gaseous LBC are the same as the CMAQ base case. GEOS-LBC provides both the gaseous and aerosol LBCs. GLBC-monthly is the static CLBC generated from the monthly mean GCCM results. The AOT-NLBC is the same as GLBC-monthly except that its northern LBC is generated from the relationship of VIIRS (Visible Infrared Imaging Radiometer Suite) AOT and GEOS LBC for the wildfire intrusion events, which will be described later.

An interface between NAQFC and GEOS has been developed to transfer CLBCs. It is based on the existing Global-to-Regional interfaces developed by Tang et al (2008, 2007) for MOZART, RAQMS, and NGAC global models with the enhancement to support GEOS's NetCDF4 format, vertical layers and chemical species. The interface includes two major functions: spatial mapping and species mapping. Spatially, GEOS's concentrations from its 576×361 grid in the 0.625º×0.5º

https://doi.org/10.5194/acp-2020-587
Preprint. Discussion started: 5 August 2020

Atmospheric Chemistry and Physics Discussions

horizontal resolution with 72 vertical layers are 3-dimensionally interpolated into CMAQ's CONUS lateral boundary periphery in the 12km horizontal resolution. Since the different chemical mechanisms have been employed in global chemical transport models and CMAQ, the species mapping are required to link both models.

2.1 Gaseous Species Mapping

The GCCM outputs 122 gaseous chemical species and 15 aerosol species. For the species such as O_3, CO, NO, and NO_2, an explicit one-on-one mapping can be achieved. However, some voltaic organic compounds (VOCs) need special treatment during the conversion as GCCM uses different lumping approaches from the CMAQ CB05tucl (carbon bond 5 mechanism with toluene and chloride species). Table 2 lists the VOC species map used to convert GCCM's gaseous species to CMAQ's CB05tucl species. Two methods were employed for VOCs' speciation mapping: one was based on the carbon bond structure, e.g. ALK4 → 4 PAR (Table 2), and the other was based on the similarity of the reactions. For instance, in the GEOS, the products of isoprene reaction with NO3 are lumped into INO2.

$$\text{ISOP} + \text{NO3} \rightarrow \text{INO2}$$

The corresponding CB05tucl reaction represents it as

$$\text{ISOP} + \text{NO3} = 0.200*\text{ISPD} + 0.800*\text{NTR} + \text{XO2} + 0.800*\text{HO2} + 0.200*\text{NO2} + 0.800*\text{ALDX} + 2.400*\text{PAR}$$

Therefore, the GEOS species of INO2 should be split into seven CB05tucl species with the corresponding factors, respectively (Table 2). Some species are represented explicitly in the GEOS, such as methyl vinyl ketone (MVK), which is lumped in CB05tucl's isoprene product (ISPD). Thus we can map GEOS MVK directly into the CB05tucl's ISPD. Some GEOS species can also be mapped to the CB05 species based on their carbon bonds, e.g. R4N2 (GEOS's C4-5 alkyl nitrates) can be mapped to NTR + 2.0 PAR in the CB05tucl mechanism.

2.2 Aerosol Species Mapping

Both GEOS and NGAC use the GOCART aerosol scheme though in different versions (Bian et al, 2017 and Colarco et al 2010, respectively), and GEOS has additional species of ammonium and 3-bin nitrates (NO3an1, NO3an2 and NO3an3). Table 3 lists the aerosol species mapping from GEOS aerosols to CMAQ Aero6 species used in this study. GEOS aerosols have fixed size bins defined by their diameters, while CMAQ aerosols use 3 size modes: Aitken (ATKN), accumulations (ACC) and coarse (COR) modes (i, j, k modes) (Appel et al., 2010) and each size mode has its own lognormal size distribution (Whitby and McMurry, 1997). To convert the aerosol species from GEOS to CMAQ's Aero6, we need to consider not only the aerosol composition and the conversion from GEOS size bins to the CMAQ size modes, but also the size distribution within each CMAQ size mode that is controlled by the CMAQ aerosol number

https://doi.org/10.5194/acp-2020-587
Preprint. Discussion started: 5 August 2020


Atmospheric Chemistry and Physics Discussions

concentrations (the 3rd column of Table 3). Dust is converted to AOTHRJ (other unreactive aerosol in accumulation mode) and ASOIL (soil particles in coarse mode). They do not participate in any aerosol reaction, but are just counted in total PM2.5 and PM10. Although the CMAQ Aero6 has explicit elemental ions, like Ca and Mg, which are possible dust ingredients, we do not consider the reaction effect due to these ions. Tang et al. (2004) studied the dust outflow during ACE-Asia field experiment and found that only small portion of cations in dust particles are available for aerosol uptake or reactions, which was nearly none for aged dust air masses.

3. Case Studies for the LBCs in Summer 2015

To evaluate the impact of LBCs on the model simulations, we chose the period that covered the intrusion events. During summer 2015, two intrusion events occurred in the Southeastern USA and Northern USA, respectively. The Southeastern intrusion was brought by the long-range transported dust storm from the Saharan desert. The northern intrusion was caused by the Canadian wildfire and its southward transport into the CONUS. Figure 1 shows the aerosol optical thickness retrieved from Suomi-NPP satellite's VIIRS instrument from later June to early July, 2015, which highlights these two intrusion events.

3.1 Dust Storm Events in Summer 2015

As shown in Figure 1, a dust storm was originated from the Saharan desert, and brought to the Southeastern USA via the trans-Atlantic transport. The two global models, GEOS and NGAC, captured this dust intrusion, and provided the signals of aerosol increments via their CLBCs to NAQFC. Figure 2 shows the NAQFC domain and its southeastern corner covered the Bermuda and Bahamas Islands. Figure 3 shows the corresponding three LBCs for ASOIL and AOTHRJ along the model's boundary locations on July 2, 2015 as the GOCART dusts have been mapped into two CMAQ aerosol species (Table 3). The base run (CMAQ_BASE) used the clean background for these two CMAQ aerosols. All three LBCs show enhanced ASOIL and AORTHJ near the domain's southeastern corner and central Southern boundary. The GLBC-Monthly is the monthly average of GEOS-LBC for July 2015, and has the lowest increments for the two types of aerosols. The two dynamic LBCs, the GEOS-LBC and NGAC-LBC, show the similar aerosol increments over similar locations. However, the NGAC aerosols tended to spread broader than those of the GEOS-LBC, especially for ASOIL, which could reach above the altitude of 10km with concentrations > 5 $\mu g/m^3$ (Figure 3e). The NGAC-LBC also showed some signals over the western boundary, where the GEOS-LBC did not show any dust-related aerosols. Another difference between these two LBCs is their ratio of AORTHJ versus ASOIL. The dynamic NGAC-LBC had the higher ASOIL, the coarse-mode dust, than that of GEOS-LBC (Figure 3a, 3e), but its AOTHRJ (accumulation-mode dust) was lower than the latter (Figure 3b, 3f), especially over the central southern boundary, where the GEOS-LBC had AOTHRJ up to 30 $\mu g/m^3$. It implied that these two global models could have some difference on their dust size distributions, besides their difference on transport patterns due to their dynamics or physics.

https://doi.org/10.5194/acp-2020-587
Preprint. Discussion started: 5 August 2020


Atmospheric Chemistry and Physics Discussions

Figure 4 shows the regional PM2.5 comparisons with the observations from the U.S.EPA AIRNow stations. The CMAQ_Base represented the clear background situation, which obviously missed this dust intrusion event, and underestimated the PM2.5 over Southern and Southeastern USA. The two dynamical LBCs, GEOS-LBC and NGAC-LBC, well captured the intrusion signals and yielded the best results. Their performance were similar in Florida, which was much better than the CMAQ_BASE, but still underpredicted the PM2.5 over central Florida. Over Texas, the further downwind region of this dust intrusion, the GEOS-LBC yielded broader and higher PM2.5 increments than that of the NGAC-LBC, and agreed better with observations, though it had some overprediction over Northern Texas. The monthly averaged GLBC-Monthly had moderate PM2.5 enhancement and still underestimated the dust intrusion, ranking between the CMAQ_BASE and two dynamic LBCs. Figure 5 shows a similar story for the scenario of 3 days later. The GEOS-LBC yielded the best overall results, though it still underpredicted the PM2.5 over Florida and Northern Texas. Figure 6 illustrates the time-series comparison for this dust intrusion case over Florida and Texas. In general, the performance ranking of these simulations had GEOS-LBC > NGAC-LBC > GLBC-Monthly > CMAQ_Base, except the NGAC-LBC's underprediction over Florida in June. Even though these dynamic LBCs had overall better results than the static LBCs, they still missed some intrusion peaks, such as June 30th over Texas, and had some inconsistent time-variation patterns compared with the observations, e.g. July 1st over Florida, and July 8th over Texas. The two dynamic LBCs had similar performance over Florida in July. However, in the further downwind area, such as Texas, the GEOS-LBC showed better result than that of the NGAC-LBC. These model-observation comparisons showed the advantage of the dynamic LBCs for capturing intrusion events. It should be noted that the PM2.5 spike at July 4th night (July 5th in UTC time) was not related to the dust intrusion, but caused by firework emissions at night for the Independence Day, and that emission was not included in our anthropogenic emission inventory.

3.2 The Wildfire Event in Summer 2015

During the same period of summer 2015, a wildfire event occurred in Canada and the biomass burning plume was transported to the United States and affected the Northern USA, as shown in Figure 1. Differing from the dust storm intrusion that mainly affected the particle matter (PM) concentrations, the biomass burning plumes also included gaseous pollutants, such as enhanced level of CO, NO_x, and volatile organic compounds (VOCs), which could contribute to the photochemical generation of ozone. For aerosol species, the biomass burning airmass were mainly represented with the enhancement of elemental carbon (EC) and primary organic carbon (POC), or AECJ and APOCJ in CMAQ (Table 3). Figure 7 shows a snapshot of the LBCs along the domain boundaries for AECJ+APOCJ and CO. The GEOS-LBC showed the highest aerosol and CO concentrations with AECJ+APOCJ up to 300 $\mu g/m^3$, and CO up to 3000 ppbV along the domain's northern boundary. Another important feature of GEOS-LBC was that its CO enhancement appeared at elevated altitudes up to 12km (Figure 7b). The monthly averaged GLBC-monthly showed the similar features to the GEOS-LBC, but with much lower

https://doi.org/10.5194/acp-2020-587
Preprint. Discussion started: 5 August 2020


Atmospheric Chemistry and Physics Discussions

concentrations (Figure 7c, 7d). The NGAC-LBC had the similar AECJ+APOCJ profiles to GLBC-monthly, and it used the static profile CO boundary condition (same as the CMAQ_base) that did not reflect the wildfire influence (Figure 7e, 7f).

As enhanced gaseous pollutants brought by the full-chemistry LBCs would increase the photochemical generation of ozone, the higher ozone also appeared along the northcentral boundary (Figure S1a, S1b), where the GEOS-LBC showed 10 ppbv or higher O_3 concentration below 4km more than those in the static NGAC-LBC or CMAQ_Base (Figure S1c). The wildfire induced ozone enhancement appeared not only in the lower troposphere, but also at higher altitudes, e.g. 11km, where the high ozone did not solely come from the stratosphere (Figure S1a). Figure S2 showed the other species from GEOS-LBC, in which the short-lived NOx had < 1 ppbv increment (Figure S2a) due to the wildfire intrusion. However, its NOz (sum total of all NOx oxidation products, NOz=NOy-NOx) enhancement could be up to 30 ppbv (Figure S2b) along the northern boundary around 10-12km altitude, where the CO increment also co-existed (Figure 7b). NOz is a good indicator for NOx's photochemical formation of ozone (Sillman et al., 1997) and the O3/NOz ratio is used as the ozone photochemical efficiency per NOx. The CO and NOz appearance in the high altitudes reflected that the GEOS injected the wildfire emissions to upper troposphere from the strong fire case. Besides these species, the VOCs also showed increment due to the wildfire plume, such as ethane (Figure S2c) and HCHO (S2d). HCHO is short-lived species, and an indicator of VOC oxidation (Arlander et al., 1995). Considering the magnitudes of CO, VOC and NOx increments in this LBC, the GEOS-LBC mainly provided the VOC and CO rich airmass with limited NOx to the regional CMAQ model. When this kind of airmass arrived at NOx-rich region, such as the urban areas, it would contribute to the photochemical generation of ozone.

Figure 8 shows the comparison of PM2.5 predictions at 18 UTC, 07/03/2015. The CMAQ_Base missed the intruded biomass burning plumes and the corresponding high PM2.5 over the North/South Dakoda, Montana, and Minnesota (Figure 8a). The GEOS-LBC predicted the highest PM2.5 increment (up to 200 $\mu g/m^3$) over these states, and agreed best with the AIRNow observation, though it still had some missed predictions, including both underprediction and overprediction (Figure 8b). The dynamic NGAC-LBC and static GLBC-Monthly showed the similar PM2.5 enhancements over the affected states, but almost one order of magnitude lower than that of GEOS-LBC. Figure 9 shows the similar predictions but for ozone. Again, the GEOS-LBC yielded the highest ozone increment due to its relatively high ozone concentration from the wildfire plume, which, however, still underestimated the ozone over North Dakota (Figure 9b). The monthly mean LBC, GLBC-Monthly, systemically underestimated the ozone over these regions. The CMAQ_Base and NGAC-LBC used the same static gaseous LBC, including that for ozone, and they underestimated more. Since the NGAC-LBC had more wildfire-induced aerosol loading than that of CMAQ_Base, the former's photolysis rate was lower than the latter. As both of NGAC-LBC and CMAQ_Base carried the "clean" airmass with low-concentration ozone precursors over the Northern USA, the photolysis reduction due to

https://doi.org/10.5194/acp-2020-587
Preprint. Discussion started: 5 August 2020


Atmospheric Chemistry and Physics Discussions

aerosols mainly led to the reduced ozone's photolytic destruction, such as $O_3 \rightarrow O^1D + O_2$ or $O_3 \rightarrow O^3P + O_2$, instead of its photochemical generation. For the same reason, ozone's lifetime in winter is longer that in summer (Janach, 1989). On the contrary, over polluted regions, the photolysis reduction would cause lower ozone concentration by limiting its photochemical production. Overall, this effect of photolysis rates on ozone was relatively small. Figure 10 shows the time-series comparison over the Northcentral and Northeastern USA for PM2.5 and ozone. Except the systematic PM2.5 underestimation on the night of July 4th due to the missed firework emissions, the GEOS-LBC showed better PM2.5 prediction than the others, especially from June 29 to July 2 over Northern USA. It should be noted that this run was still not perfect, as it underestimated PM2.5 in the further downwind, the Northwestern USA. The GEOS-LBC also better captured the peak ozone concentrations, e.g. July 1st and July 2nd, though it sometimes overpredicted ozone especially during nighttime. The small ozone difference between the CMAQ_Base and NGAC-LBC reflected the impact of wildfire aerosols on photolysis rates, which was very small with regional averages < 1 ppbv throughout this period (Figure 9c, 9d).

3.3 Statistics and Discussion

Table 4 summarizes the PM2.5 statistic results during the two weeks of the intrusion events over the CONUS domain and sub-regions. The dynamic LBCs, GEOS-LBC and NGAC-LBC, showed significant improvements for almost all scores over these regions as compared to the CMAQ_Base. The GLBC-Monthly was also better than the base case, though its improvement on correlation coefficient R and index of agreement (IOA) was relatively moderate compared to the dynamic LBCs, as its time-averaging removed the temporal variations. For the further downwind regions of the intrusion events, the LBCs' improvement depended on the regional characteristics of pollutant concentrations. For instance, since the Rocky Mountain region was relatively clean due to its low local PM sources, the external influence weighed more, and the LBCs also showed more significant impact there. Over more polluted regions where relatively strong local PM sources existed, such as Pacific Coast and Northeastern USA, the LBCs mainly changed the background concentration for PM2.5, and their impact on R or IOA were very limited. Overall, the GEOS-LBC yielded the best prediction by reducing the mean bias (MB), root mean square error (RMSE) and increasing the R and IOA. The other dynamic LBC, NGAC-LBC, ranked second. All these LBCs showed better performance than the base case for PM2.5 prediction.

Table 5 shows the similar statistics for ozone. It should be noted that the CMAQ_Base had a systemic O_3 overprediction, especially over the Southcentral region, which affected the improvement of LBCs. Differing from PM2.5, ozone had strong diurnal variation during the summertime, which made the LBCs' impact on R and IOA less significant. It should also be noted that the NGAC-LBC did not change any precursor concentrations related to ozone production, and just affect the ozone formation by reducing photolysis rates. Therefore, as compared to CMAQ_Base, the NGAC-LBC had very weak influence on O_3 by generally reducing the regional O_3 by around 0.2 ppbV, and had almost no impact on R or IOA. The

https://doi.org/10.5194/acp-2020-587
Preprint. Discussion started: 5 August 2020


Atmospheric Chemistry and Physics Discussions

GEOS-LBC tended to increase ozone concentrations in most regions, except the Southcentral USA, where the GEOS-LBC showed general improvement for all scores. It had the weakest impact on ozone over Pacific Coast and Rocky Mountain regions, or the farther downstream areas. The GLBC-monthly had the highest ozone increment over most region except the Southcentral, and its RMSE was also slightly higher. This result showed that removing temporal variation of a LBC might not affect ozone prediction linearly. Except the mean bias, the GEOS-LBC got better scores over most regions, though the improvement on O_3 was not as significant as that on PM2.5. As discussed above, the LBC impact on ozone inside the domain was realized through changing inflow concentration of O_3 itself and/or O_3 precursors, such as NOx, VOC or CO. The distance or depth of LBC's effective impact from the inflow boundary depended on the lifetime of these species. All these species have longer lifetime in winter than those in summer. Our other study showed that the LBC's impact on ozone in winter was stronger than that in summer.

Figure 11 further illustrated the impact of LBCs (using GEOS-LBC as an example) on prediction statistics and their relations to the distance from the domain boundary during the intrusion events: Southern USA for the Saharan dust intrusion (Figure 11 a,b), and Northern USA for the wildfire intrusion case (Figure 11 c,d). As discussed before, the CLBC has two roles in the regional predictions: provide a constraint for background concentrations, represented by the mean biases, and introduce the variational external influence, represented by the correlation coefficients. Both the background and the variation of CLBC affected the RMSE of predictions. Over the Southern USA, the Saharan dust storm intruded through States of Texas and Louisiana, or -100°W to -86°W, and moved northwardly (Figure 4). Figure 11a showed that the GEOS-LBC's improvement on the correlation coefficient R for the PM2.5 prediction reached the highest near the southernmost near-boundary region, and gradually reduced along the latitude for the inland region. On the other hand, the corresponding MB improvement for PM2.5 did not show significant reduction along the distance from the influenced boundary. The second role of the CLBC, constraining background concentrations for PM2.5, can affect farther inside of the domain. The PM2.5 RMSE change reflected the combined changes of MB and R, and its improvement brought by the GEOS-LBC also reduced along the distance from the influenced boundary since the MB improvement did not vary much and the change trend of RMSE mainly followed the change of R along the latitude. The spatial variations of O_3 statistics differed obviously from those of PM2.5 statistic (Figure 11b), and the most significant R's improvement for O_3 was not near boundary, but in the some middle latitudes (29°N to 32°N) before reducing in the farther inland. Its MB and RMSE improvements had the similar spatial variations, and they were the highest near the boundary and reduced along the latitude increment. One reason for this difference between PM2.5 and O_3 statistics is that the O_3 usually has stronger local diurnal variation in summer driven by the photochemical activities, and that influence on R could be stronger than the external influence over polluted areas. So, for this event in which O_3 was not the key species, the GEOS-LBC's influence on O_3 prediction was mainly about changing its background concentration. Figure 11b also showed that the O_3 MB of the GEOS-LBC run could

https://doi.org/10.5194/acp-2020-587
Preprint. Discussion started: 5 August 2020


Atmospheric Chemistry and Physics Discussions

change from lower to higher than of that the reference run (CMAQ_base) along with the latitudinal increment. Although the ozone concentration of the GEOS-LBC over the south boundary was lower than that of the CMAQ_base in low altitudes, it had higher ozone values in the altitudes higher than 14000 m (Figure S1). That high ozone concentration could reach surface after a certain distance of downward transport in the model system with strong vertical mixing (Tang et al., 2009), which resulted in the higher ozone MB of the GEOS-LBC over the deeper inland region.

For the wildfire intrusion event over Northern USA, the PM2.5 statistical difference between GEOS-LBC and CMAQ_Base showed the similar spatial distribution to the dust intrusion event: R and RMSE improvements of the GEOS-LBC appeared the most significant near the boundary, and reduced along the distance from the boundary, and its MB difference could be maintained deeper inland (Figure 11c). For the O_3 statistic, the difference between GEOS-LBC and CMAQ_Base became more complex as the wildfire plume also contained the intrusion influence for O_3 and its precursors. The GEOS-LBC run generally yielded higher O_3, which exaggerated the existing overprediction bias near the boundary, but helped correct the underprediction bias when moving farther inland (Figure 11d). The biggest difference of O_3 MB also appeared in the middle latitude as the O_3 precursors brought by the full-chemistry LBC took time to contribute to O_3 photochemical formation. The spatial variation of O_3 RMSE difference was similar to that of O_3 MB except for the farther inland region with latitude < 43°N where the GEOS-LBC did not improve the RMSE. The similar issue also appeared for the R difference for the region south of 46°N, implying that the wildfire plume represented by the GEOS-LBC could introduce some spatial or temporal biases for O_3 precursors.

4. AOT Derived Lateral Boundary Conditions

The dynamic LBC, such as GEOS-LBC, showed overall better prediction for the intrusion events by capturing the external influence at right time over right locations. However, this full-chemistry LBC sometimes is not easy to obtain, especially for the near-real-time forecast. Its event-depended emissions, such as the wildfire emission, also need some time to get relatively accurate estimation, and their impacts on regional domain could lag behind the scene for the forecast. In order to get the intrusion influence when the real-time LBC was not available, we tested the method of developing an alternative LBC based on the historical data with certain indicators. Here we focused on the wildfire intrusion, since it was more difficult to capture the sudden outbreak of wildfire signal than the long-range transport dust intrusion. In addition, the operational NGAC dust forecast has been available to NAQFC (Wang et al, 2018).

4.1 Development of the LBC with VIIRS AOT for Wildfire Plumes

Figure 1 showed that the VIIRS retrieved AOT well reflected the wildfire intrusion with broad spatial coverage, superior to the sporadic surface stations along the north boundary of the CONUS domain. So VIIRS AOT could be used as an indicator for wildfire plumes. Figure S3

https://doi.org/10.5194/acp-2020-587
Preprint. Discussion started: 5 August 2020


Atmospheric Chemistry and Physics Discussions

showed the comparison of extracted VIIRS AOT versus GEOS CO and EC column loading along the northern boundary for June-July, 2015, with their correlation coefficients R > 0.5. The regression relationship derived out of Figure S3 can then be used to resample the historical GEOS LBC data to derive a new LBC for wildfire intrusion events when the corresponding AOT is available. The domain's northern boundary was relatively clean in most time of the summer, unless the wildfire events occurred. During the June and July 2015, the VIIRS AOT data was available once or twice per day around local noontime under cloud-free condition. To get more VIIRS AOT data along the northern boundary, we relaxed the influencing distance up to 300 km when pairing the VIIRS AOT geolocation and the northern boundary location with the nearest neighbor method. In this study, we paired the GEOS's northern LBC (NLBC) for 18UTC with the daily VIIRS AOT along the same location, and made an average of the whole column with AOT interval of 0.2 to build a LBC database sorted in AOT. We only chose to resample the LBC for primarily emitted species from the wildfire sources, including POC, EC, CO, NOx, and two NOz species: PAN and HNO_3, but did not include the ozone LBC. When the VIIRS AOT for the new events are available for NLBC, the whole-column species concentration data from that database are chosen to form the new LBC based on the VIIRS AOT value in the nearest neighbor.

4.2 A Case Study with VIIRS AOT Derived LBC in August, 2018

In the middle-later August 2018, a wildfire occurred in western Canada. Figure S4 showed that a high-pressure system controlled the western Canada, and the dry weather made the wild fire easily to spread. There were prevailing northern or northeastern wind, which brought the fire pollutants southward to affect the northwestern and northern U.S. states. Figure 12a shows the VIIRS AOT for this event with the high AOT appearing in the western Canada, the main source region, and the Northern and Northwestern USA. We used this AOT data to derive the new LBC along the northern boundary (Figure 12b, c) for CO and wildfire emitted aerosols (AECJ+APOCJ) by resampling the historical GEOS-LBC database from the Jun-Jul, 2015 period. This AOT derived northern LBC (AOT-NLBC) was updated once per day due to the VIIRS data availability, while its western, southern, and eastern boundaries came from the climatologic monthly-mean GEOS-LBC (averaged from 2011 to 2015). The AECJ+APOCJ increment of the AOT-NLBC mainly existed below 3km, but its CO enhancement could reach up to the altitude of 10km, due to the elevated CO plume in the original GEOS-LBC, e.g. Figure 7b.

Figure 13 shows the surface ozone and PM2.5 over this region one day later (08/17/2018). The CMAQ_Base underpredicted both species over this region, while the AOT-NLBC greatly reduced the underprediction with increased background concentration from the northern boundary. Since the AOT-NLBC did not include dynamic ozone LBC, its enhanced ozone concentration was mainly brought by the CO and NOx increments from the northern boundary, which sometimes caused the overprediction over further downwind areas, such as Colorado. Overall, the AOT-NLBC showed better PM2.5 prediction over Southwestern Canada and Northwestern USA with its higher background concentrations.

https://doi.org/10.5194/acp-2020-587
Preprint. Discussion started: 5 August 2020


Atmospheric Chemistry and Physics Discussions

Figure 14 shows the corresponding time-series comparison over EPA region 8 (states of Montana, North and South Dokotas, Wyoming, Colorado, and Utah) and region 10 (states of Washington, Idaho, and Oregon). Both observed and predicted ozone showed strong diurnal variation. The AOT-NLBC showed better skill on capturing daytime ozone maximum, and was about 5-10 ppbv higher than the CMAQ_base prediction, though it tended to overpredict ozone at night, especially over the region 8. For PM2.5, the observation clearly showed two peaks related to wildfire plumes over two regions: 08/19-08/21 and 08/24-08/25 for EPA region 8; 08/14-08/17 and 08/19-08/22 for EPA region 10. Without the boundary influence, the CMAQ_Base missed all these PM2.5 peaks even though it had the same inside-domain wildfire emissions. AOT-NLBC successfully captured these intrusion signals, though overpredicted PM2.5 before 08/18 over EPA region 8. This result showed that the alterative LBC could be useful for capturing the key intrusion signals in case the global LBC was not available. This alternative approach was especially important for the forecast as the satellite AOT can be obtained in near-real-time. In this case study of summer 2018, the wildfire events were similar to the wildfire case occurred in summer 2015, which made the quantitative derivation of LBC possible.

5. Conclusion

In this study, we examined the influence of the CLBC on our regional air quality prediction, verified with surface ozone and PM2.5 monitoring observations. We developed the full-chemistry mapping table from the global model GEOS to CMAQ's CB05-Aero6 species. The GEOS dynamic LBC showed the overall best score when comparing with the surface observations during the June-July 2015 while Saharan dust intrusion and Canadian wildfire events occurred. The base simulation (CMAQ_Base) ranked last as it missed all these external influences. The NGAC-LBC only considered the GOCART aerosols, and had the good performance for capturing the dust storm intrusion but missed the ozone enhancement due to the Canadian fire events. The LBC influences on the model performance depended on not only the distance from the inflow boundary but also species and their regional characteristics, as the LBCs' influence on ozone and PM2.5 differed significantly. During the studied events of summer 2015, The CLBCs affected both PM2.5 mean background concentration and its temporal/spatial variation. Their influences on PM2.5's correlation coefficient R mainly appeared near inflow boundary, and reduced along with the distance from the boundary. However, their influence on PM2.5 background concentration could be kept in the further inside domain. The CLBCs' influence on ozone could be more complex, and affected by the boundary inflow of ozone and/or its precursors, and downward transport from the upper troposphere. In this study, the influences with temporal/spatial variation were mainly shown in the aerosol dynamic LBC, e.g. the GEOS-LBC or NGAC-LBC. All other LBCs mainly changed the background concentrations and shifted the mean bias of the corresponding predictions.

https://doi.org/10.5194/acp-2020-587
Preprint. Discussion started: 5 August 2020


Atmospheric Chemistry and Physics Discussions

The AOT-derived LBC can be used as an alternative method to capture the intrusion when a reliable dynamic LBC is not available. Although the VIIRS AOT was updated only once per day and the derived LBC had noisy spatial distribution, this method still showed its value to replace the static LBC in the air quality forecast. It should be noted that other indicators, such as surface monitoring data, can be also used to derive the similar LBC if the historical LBC has good correlation with these data and there are relatively dense station available near the inflow boundary. Geostationary satellites can achieve a near-real-time AOT retrieval in time interval of several minutes, which will provide a better solution for fast capturing the intrusion signals. Currently the main issue for using geostationary AOT is their relatively poor retrieval quality over high latitude or under high zenith angles. Once that issue gets resolved, its AOT can be used as an indicator to derive the LBC or even replace the LBC provided by the global models.

https://doi.org/10.5194/acp-2020-587
Preprint. Discussion started: 5 August 2020

Atmospheric Chemistry and Physics Discussions

Code and Data availability

The source code used in this study is available online at https://github.com/NOAA-EMC/EMC_aqfs (last access: 4 May 2020; NOAA-EMC, 2020). The VIIRS AOT data used here are in ftp://ftp.star.nesdis.noaa.gov/pub/smcd/VIIRS_Aerosol/npp.viirs.aerosol.data/epsaot550/. The surface AIRNow monitoring data can be obtained via https://airnow.gov.

Acknowledgements

This research was supported by National Oceanic and Atmospheric Administration (NOAA) under its Office of Weather and Air Quality program with funding number NA16OAR4590118 and NOAA National Air Quality Forecast Capability (grant # T8MWQAQ). We thank the NASA MAP program and NASA Center for Climate Simulation for support in of the GEOS GMI model.

Reference

Appel, K. W., S. J. Roselle, R. C. Gilliam, and J. E. Pleim, Sensitivity of the Community Multiscale Air Quality (CMAQ) model v4. 7 results for the eastern United States to MM5 and WRF meteorological drivers. Geosci. Model Dev., 3, 169–188, 2010.

Arlander, D.W., Brüning, D., Schmidt, U. and Ehhalt, D.H., 1995. The tropospheric distribution of formaldehyde during TROPOZ II. Journal of atmospheric chemistry, 22(3), pp.251-269.

Bey, I., D.J. Jacob, J.A. Logan, R.M. Yantosca, Asian chemical outflow to the Pacific in spring: origins, pathways, and budgets. *J. Geophys. Res.*, 106 (D19), pp. 23097-23113, 2001.

Bian, H., M. Chin, D. A. Hauglustaine, M. Schulz, G. Myhre, S. E. Bauer, M. T. Lund, V. A. Karydis, T. L. Kucsera, X. Pan, A. Pozzer, R. B. Skeie, S. D. Steenrod, K. Sudo, K. Tsigaridis, A. P. Tsimpidi, and S. G. Tsyro (2017), Investigation of global particulate nitrate from the AeroCom phase III experiment Atmos. Chem. Phys., 17, 12911–12940 (https://www.atmos-chem-phys.net/17/12911/2017/).

Chin, M., Rood, R. B., Lin, S.-J., Muller, J.-F., and Thompson, A. M.: Atmospheric sulfur cycle simulated in the global model GOCART: Model description and global properties, *J. Geophys. Res.*, 105, 24671–24687, doi:10.1029/2000JD900384, 2000.

Chin, M., Ginoux, P., Kinne, S., Torres, O., Holben, B. N., Duncan, B. N., Martin, R. V. , Logan, J. A., and Higurashi, A.: Tropospheric aerosol optical thickness from the GOCART model and comparisons with satellite and Sun photometer measurements, *J. Atmos. Sci.*, 59, 461–483, 2002.

Colarco, P., da Silva, A., Chin, M., Diehl, T., Online simulations of global aerosol distributions in the NASA GEOS-4 model and comparisons to satellite and ground- based aerosol optical depth. J. Geophys. Res. 115, D14207. https://doi.org/ 10.1029/2009JD012820. 2010.

Janach, W.E., 1989. Surface ozone: trend details, seasonal variations, and interpretation. *Journal of Geophysical Research: Atmospheres*, 94(D15), pp.18289-18295.

Lee, P., J. McQueen, I. Stajner, J. Huang, L. Pan, D. Tong, H.-C. Kim, Y. Tang, S. Kondragunta, and M. Ruminski, NAQFC developmental forecast guidance for fine particulate matter (PM2. 5), Weather and Forecasting, 32: 343-60. doi:10.1175/waf-d-15-0163.1, 2017.

https://doi.org/10.5194/acp-2020-587
Preprint. Discussion started: 5 August 2020

Atmospheric Chemistry and Physics Discussions

Lu, C.-H., da Silva, A., Wang, J., Moorthi, S., Chin, M., Colarco, P., Tang, Y., Bhattacharjee, P. S., Chen, S.-P., Chuang, H.-Y., Juang, H.-M. H., McQueen, J., and Iredell, M.: The implementation of NEMS GFS Aerosol Component (NGAC) Version 1.0 for global dust forecasting at NOAA/NCEP, *Geosci. Model Dev.*, 9, 1905-1919, https://doi.org/10.5194/gmd-9-1905-2016, 2016.

Molod, A., L. Takacs, M. Suarez, J. Bacmeister, I.-S. Song, and A. Eichmann, The GEOS Atmospheric General Circulation Model: Mean Climate and Development from MERRA to Fortuna. Technical Report Series on Global Modeling and Data Assimilation, 28, 2012.

Pan, L., Tong, D., Lee, P., Kim, H.C. and Chai, T.. Assessment of NOx and O_3 forecasting performances in the US National Air Quality Forecasting Capability before and after the 2012 major emissions updates. *Atmospheric Environment*, 95, pp.610-619, 2014.

Pierce, T., C. Geron, L. Bender , R. Dennis, G. Tonnesen, and A. Guenther A, Influence of increased isoprene emissions on regional ozone modeling. *J. Geophys. Res.* 103:25611–25629, 1998.

Mathur, R., Xing, J., Gilliam, R., Sarwar, G., Hogrefe, C., Pleim, J., Pouliot, G., Roselle, S., Spero, T.L., Wong, D.C. and Young, J., Extending the Community Multiscale Air Quality (CMAQ) modeling system to hemispheric scales: overview of process considerations and initial applications. Atmospheric chemistry and physics, 17, p.12449. doi: 10.5194/acp-17-12449-2017, 2017

Sarwar, G., Luecken, D., and Yarwood, G.: Chapter 2.9 Developing and implementing an updated chlorine chemistry into the community multiscale air quality model, in: Air Pollution Modeling and Its Application XVIII, edited by: Borrego, C. and Renner, E., vol. 6 of Developments in Environmental Science, 168– 176, Elsevier, Amsterdam, the Netherlands, doi:10.1016/S1474- 8177(07)06029-9, 2007.

Sillman, S., He, D., Cardelino, C. and Imhoff, R.E., The use of photochemical indicators to evaluate ozone-NOx-hydrocarbon sensitivity: Case studies from Atlanta, New York, and Los Angeles. *Journal of the Air & Waste Management Association*, 47(10), pp.1030-1040, 1997.

Sonntag, D. B., R. W. Baldauf, C. A. Yanca and C. R. Fulper, Particulate matter speciation profiles for light-duty gasoline vehicles in the United States, *Journal of the Air & Waste Management Association*, 64:5, 529-545, DOI:10.1080/10962247.2013.870096, 2014.

Strode S.A., J.R. Ziemke, L.D. Oman, L.N. Lamsal, M.A. Olsen, J. Liu, Global changes in the diurnal cycle of surface ozone, *Atmospheric Environment*, 199, 323-333, https://doi.org/10.1016/j.atmosenv.2018.11.028, 2019.

Tanaka, P. L., Allen, D. T., McDonald-Buller, E. C., Chang, S., Kimura, Y., Mullins, C. B., Yarwood, G., and Neece, J. D.: Development of a chlorine mechanism for use in the carbon bond IV chemistry model, *J. Geophys. Res.-Atmos.*, 108, 4145, doi:10.1029/2002JD002432, 2003.

Tang Y., Carmichael G. R., Thongboonchoo N., Chai T., Horowitz L.W., Pierce R. B., Al-Saadi J. A., Pfister G., Vukovich J. M., Avery M. A., Sachse G. W., Ryerson T. B., Holloway J. S., Atlas E. L., Flocke F. M., Weber R. J., Huey L. G., Dibb J. E., Streets D. G., and Brune W. H.: Influence of lateral and top boundary conditions on regional air quality prediction: a multiscale study coupling regional and global chemical transport models. *J. Geophys. Res.* 112:D10S18. doi:10.1029/2006JD007515, 2007.

Tang, Y., Lee, P., Tsidulko, M., Huang, H.C., McQueen, J.T., DiMego, G.J., Emmons, L.K., Pierce, R.B., Thompson, A.M., Lin, H.M. and Kang, D.: The impact of chemical lateral

https://doi.org/10.5194/acp-2020-587
Preprint. Discussion started: 5 August 2020

boundary conditions on CMAQ predictions of tropospheric ozone over the continental United States. *Environmental Fluid Mechanics*, 9(1), pp.43-58, DOI:10.1007/s10652-008-9092-5, 2009

Wang, J., Bhattacharjee, P.S., Tallapragada, V., Lu, C.H., Kondragunta, S., da Silva, A., Zhang, X.Y., Chen, S.P., Wei, S.W., Darmenov, A.S. and McQueen, J.: The implementation of NEMS GFS Aerosol Component (NGAC) Version 2.0 for global multispecies forecasting at NOAA/NCEP-Part 1: Model descriptions. Geosci. Model Dev., 11, 2315–2332, https://doi.org/10.5194/gmd-11-2315-2018, 2018

Whitby, E. R., and P. H. McMurry, Modal aerosol dynamics modeling. Aerosol Science and Technology 27: 673-688, 1997

Whitten, G. Z., Heo, G., Kimura, Y., McDonald-Buller, E., Allen, D. T., Carter, W. P., and Yarwood, G.: A new condensed toluene mechanism for Carbon Bond: CB05-TU, *Atmos. Environ.*, 44, 5346–5355, doi:10.1016/j.atmosenv.2009.12.029, 2010.

Yarwood, G., S. Rao, M. Yocke, and G. Whitten. Updates to the Carbon Bond Chemical Mechanism: CB05, Technical Report RT-0400675 ENVIRON International Corporation Novato, CA, USA. 2005.

https://doi.org/10.5194/acp-2020-587
Preprint. Discussion started: 5 August 2020

Atmospheric Chemistry and Physics Discussions

Table 1 . CLBC runs conducted in this study

Runs	Aerosol LBC	Gaseous LBC	Temporal Resolution
CMAQ_Base	static clean background	GEOS-Chem 2006 with O_3 limit ≤ 100 ppbV	static monthly mean
GEOS-LBC	full aerosol	full chemistry	3 hours
GLBC-Monthly	full aerosol	full chemistry	static monthly mean
NGAC-LBC	GOCART simple aerosol	GEOS-Chem 2006 with O_3 limit ≤ 100 ppbV	3 hours
AOT-NLBC	AOT derived Northern LBC (NLBC) for EC and POC	AOT derived NLBC for CO, NOx, PAN, and HNO_3	24 hours for derived NLBC; static monthly mean for all others

https://doi.org/10.5194/acp-2020-587
Preprint. Discussion started: 5 August 2020

Atmospheric Chemistry and Physics Discussions

Table 2. VOC species mapping table from GEOS to CMAQ CB05tucl

GEOS species (mole)	CMAQ Species (mole)
HCOOH	FACD
MO_2 (CH_3O_2)	XO_2
MP (methylhydroperoxide)	MEPX
A_3O_2 (primary RO_2 from C_3H_8: $CH_3CH_2CH_2OO$)	PAR + XO_2
ACTA (acetic acid)	AACD
ATO_2 (RO_2 from acetone: $CH_3C(O)CH_2O_2$)	2*PAR + XO_2
B_3O_2 (secondary RO_2 from C_3H_8: $CH_3CH(OO)CH_3$)	2*B_3O_2
ALK4 (C_4 or higher alkanes)	4*PAR
C_3H_8	1.5*PAR + NR
ETO_2 (ethylperoxy radical: CH_3CH_2OO)	MEO_2 + PAR
ETP (ethylhydroperoxide: CH_3CH_2OOH)	MEPX + PAR
GCO_3 (hydroxy peroxyacetyl radical: $HOCH_2C(O)OO$)	C_2O_3
GLYX (glyoxal)	FORM + PAR
GLYC (glycolaldehyde: $HOCH_2CHO$)	FORM + 2*PAR
GP (peroxide from GCO_3: $HOCH_2C(O)OOH$)	ROOH
GPAN (Peroxyacylnitrate: $HOCH_2C(O)OONO_2$)	PANX
HAC (hydroxyacetone: $HOCH_2C(O)CH_3$)	2*PAR
IALD (hydroxy carbonyl alkenes from isoprene)	ISOPX
IAO_2 (RO_2 from isoprene oxidation products)	$ISOPO_2$
IAP (peroxide from IAO_2)	ROOH
INO_2 (RO_2 from ISOP+NO_3)	0.2*ISPD + 0.8*NTR+ XO_2 + 0.8*HO_2 + 0.2*NO_2 + 0.8*ALDX + 2.4*PAR'
INPN (peroxide from INO_2)	0.2*ISPD + 0.8*NTR+ ROOH + 0.8*H_2O_2 + 0.2*PNA + 0.8*ALDX + 2.4*PAR
ISN1 (RO_2 from isoprene nitrate)	NTRI
ISNP (peroxide from ISN1)	$NTRIO_2$
KO_2 (RO_2 from C_3 or higher ketones)	XO_2 + PAR
MACR (methacrolein)	ISPD
MAN2 (RO_2 from MACR+NO_3)	0.925*HO_2 + 0.075*XO_2
MAO_3 (peroxyacyl from MVK and MACR)	$MACO_3$
MAOP (peroxide from MAO_3)	ISPD
MAP (peroxyacetic acid, $CH_3C(O)OOH$)	PACD
MCO_3 (peroxyacetyl radical)	C_2O_3
MEK (C_3 or higher ketones)	4*PAR
MRO_2 (RO_2 from MACR+OH)	0.713*XO_2 + 0.503*HO_2
MRP (Peroxide from MRO_2)	ROOH
MVK (methylvinylketone)	ISPD
MVN2 (RO_2 from MVK+NO_3)	0.925*HO_2 + 0.075*XO_2
PMN (peroxymethacryloyl nitrate)	OPEN

https://doi.org/10.5194/acp-2020-587
Preprint. Discussion started: 5 August 2020

Atmospheric Chemistry and Physics Discussions

PO_2 (RO_2 from propene)	XO_2
PP (peroxide from PO_2: HOC_3H_6OOH)	ROOH
PPN (peroxypropionyl nitrate)	PANX
PRN1 (RO2 from propene+NO_3)	XO_2
PRPE (propene)	OLE + PAR
PRPN (peroxide from PRN1)	ROOH
R4N1 (RO_2 from C_4 and C_5 alkylnitrates)	ROOH + 2*PAR
R4O2 (RO_2 from C_4 alkane)	XO_2
R4P (peroxide from R4O2)	ROOH
RA3P (peroxide from A_3O_2)	ROOH
RB3P (Peroxide from B_3O_2)	ROOH
RCHO (C_3 or higher aldehydes)	ALDX
RCO3 (peroxypropionyl radical: $CH_3CH_2C(O)OO$)	XO_2
RCOOH (C_2 or higher organic acids)	AACD
RIO1 (RO_2 from isoprene oxidation products)	ISPD
RIO2 (RO_2 from isoprene)	$ISOPO_2$
RIP (Peroxide from RIO_2)	ISOPX
ROH (C_2 or higher alcohols)	3*PAR
RP (peroxide from RCO_3)	ROOH
VRO_2 (RO_2 from MVK+OH)	$ISOPO_2$
VRP (peroxide from VRO_2)	ROOH
ACET (acetone)	3*PAR

https://doi.org/10.5194/acp-2020-587
Preprint. Discussion started: 5 August 2020

Atmospheric Chemistry and Physics Discussions

Table 3. Aerosol species mapping table from GEOS to CMAQ Aero6 ("D" represents the diameter of GEOS aerosol bin)

GEOS Aerosol (μg/m^3)	**CMAQ Aerosol Mass Concentration (μg/m^3)**	**CMAQ Aerosol Number Concentration (#/m^3)**
BCPHILIC	AECJ	2.72×10^7 (ACC)
BCPHOBIC	AECJ	2.72×10^7 (ACC)
OCPHILIC	APOCJ	2.72×10^7 (ACC)
OCPHOBIC	APOCJ	2.72×10^7 (ACC)
SO4	ASO4J	2.72×10^7 (ACC)
NH4a	ANH4J	2.72×10^7 (ACC)
NO3an1 (mean D=0.5μm)	ANO3J	2.72×10^7 (ACC)
NO3an2 (mean D=4.2μm)	0.8*ANO3J + 0.2 *ANO3K	5.4×10^6(ACC) + 1.2×10^4(COR)
NO3an2 (mean D=15μm)	ANO3K	6×10^3(COR)
DU001 (D: 0.2 – 2 μm)	AOTHRJ	2.72×10^7 (ACC)
DU002 (D: 2 – 3.6 μm)	0.45*AOTHRJ+0.55*ASOIL	3.3×10^5 (ACC)+5.1×10^4(COR)
DU003 (D: 3.6 – 6 μm)	ASOIL	1.15×10^4(COR)
DU004 (D: 6 – 12 μm)	0.75*ASOIL	1.4×10^3(COR)
SS001 (D: 0.06-0.2 μm)	0.39*ANAI+0.61*ACLI	7.4×10^8(ATKN)
SS002 (D: 0.2 - 1μm)	0.39*ANAJ+0.61*ACLJ	2.72×10^7 (ACC)
SS003 (D: 1- 3μm)	0.312*ANAJ+0.488*ACLJ +0.078*ASEACAT+0.122*ACLK	1.7×10^5(ACC)+1.26×10^4(COR)
SS004 (D: 3- 10μm)	0.39*ASEACAT+0.61*ACLK	1.36×10^4 (COR)

https://doi.org/10.5194/acp-2020-587
Preprint. Discussion started: 5 August 2020

Atmospheric Chemistry and Physics Discussions

Table 4. Regional $PM_{2.5}$ statistic of the 4 simulations (CMAQ_BASE, GEOS-LBC, GLBC-Monthly and NGAC-LBC) from June 24 to July 8, 2015.

Regions	Simulations	Mean Bias ($\mu g/m^3$)	Root Mean Square Error ($\mu g/m^3$)	Correlation Coefficient, R	Index of Agreement
CONUS	CMAQ_BASE	-6.74	13.69	0.18	0.37
	GEOS-LBC	-2.96	12.16	0.37	0.55
	GLBC-Monthly	-4.10	12.39	0.27	0.41
	NGAC-LBC	-3.30	12.09	0.30	0.44
Northeastern USA	CMAQ_BASE	-5.52	10.93	0.33	0.43
	GEOS-LBC	-3.81	9.89	0.40	0.50
	GLBC-Monthly	-4.25	10.31	0.34	0.45
	NGAC-LBC	-3.70	10.05	0.35	0.46
Pacific Coast	CMAQ_BASE	-3.96	10.63	0.16	0.31
	GEOS-LBC	-2.02	10.22	0.18	0.34
	GLBC-Monthly	-1.53	10.21	0.17	0.34
	NGAC-LBC	-0.79	10.33	0.16	0.34
Southeastern USA	CMAQ_BASE	-8.18	11.35	0.14	0.44
	GEOS-LBC	-3.07	8.39	0.37	0.58
	GLBC-Monthly	-4.78	9.08	0.27	0.49
	NGAC-LBC	-3.83	8.58	0.35	0.56
Rocky Mountain States	CMAQ_BASE	-7.62	17.57	0.02	0.31
	GEOS-LBC	-3.66	15.98	0.39	0.58
	GLBC-Monthly	-5.42	16.06	0.23	0.36
	NGAC-LBC	-4.65	15.78	0.24	0.36
North Central	CMAQ_BASE	-8.32	17.63	0.25	0.38
	GEOS-LBC	-2.95	16.47	0.33	0.52
	GLBC-Monthly	-5.25	16.41	0.27	0.40
	NGAC-LBC	-4.48	15.98	0.31	0.43
South Central	CMAQ_BASE	-9.65	13.12	0.07	0.42
	GEOS-LBC	-2.00	7.79	0.51	0.69
	GLBC-Monthly	-4.73	9.45	0.24	0.48
	NGAC-LBC	-3.52	8.31	0.46	0.63

https://doi.org/10.5194/acp-2020-587
Preprint. Discussion started: 5 August 2020

Atmospheric Chemistry and Physics Discussions

Table 5. Same as Table 4 but for ozone

Regions	Simulations	Mean Bias (ppbV)	Root Mean Square Error (ppbV)	Correlation Coefficient, R	Index of Agreement
CONUS	CMAQ_BASE	2.10	12.35	0.64	0.77
	GEOS-LBC	3.47	12.01	0.68	0.79
	GLBC-Monthly	4.84	12.52	0.68	0.78
	NGAC-LBC	1.88	12.29	0.64	0.77
Northeastern USA	CMAQ_BASE	1.87	10.68	0.66	0.78
	GEOS-LBC	4.88	11.54	0.68	0.78
	GLBC-Monthly	5.60	12.02	0.66	0.76
	NGAC-LBC	1.62	10.64	0.66	0.78
Pacific Coast	CMAQ_BASE	-2.58	12.04	0.78	0.86
	GEOS-LBC	-2.16	11.83	0.79	0.87
	GLBC-Monthly	0.46	11.79	0.78	0.87
	NGAC-LBC	-2.76	12.08	0.78	0.86
Southeastern USA	CMAQ_BASE	7.26	13.66	0.59	0.68
	GEOS-LBC	7.94	13.34	0.66	0.72
	GLBC-Monthly	9.06	14.20	0.65	0.70
	NGAC-LBC	7.04	13.50	0.60	0.69
Rocky Mountain States	CMAQ_BASE	-1.91	10.61	0.67	0.80
	GEOS-LBC	-0.17	10.45	0.67	0.80
	GLBC-Monthly	1.68	10.75	0.66	0.79
	NGAC-LBC	-2.08	10.63	0.67	0.80
North Central	CMAQ_BASE	-0.47	10.78	0.65	0.78
	GEOS-LBC	2.55	11.01	0.66	0.79
	GLBC-Monthly	3.00	11.22	0.65	0.78
	NGAC-LBC	-0.75	10.76	0.65	0.78
South Central	CMAQ_BASE	13.36	17.76	0.51	0.58
	GEOS-LBC	10.90	14.71	0.68	0.68
	GLBC-Monthly	12.66	16.24	0.66	0.64
	NGAC-LBC	13.12	17.56	0.51	0.58

https://doi.org/10.5194/acp-2020-587
Preprint. Discussion started: 5 August 2020

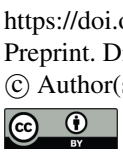

Atmospheric Chemistry and Physics Discussions

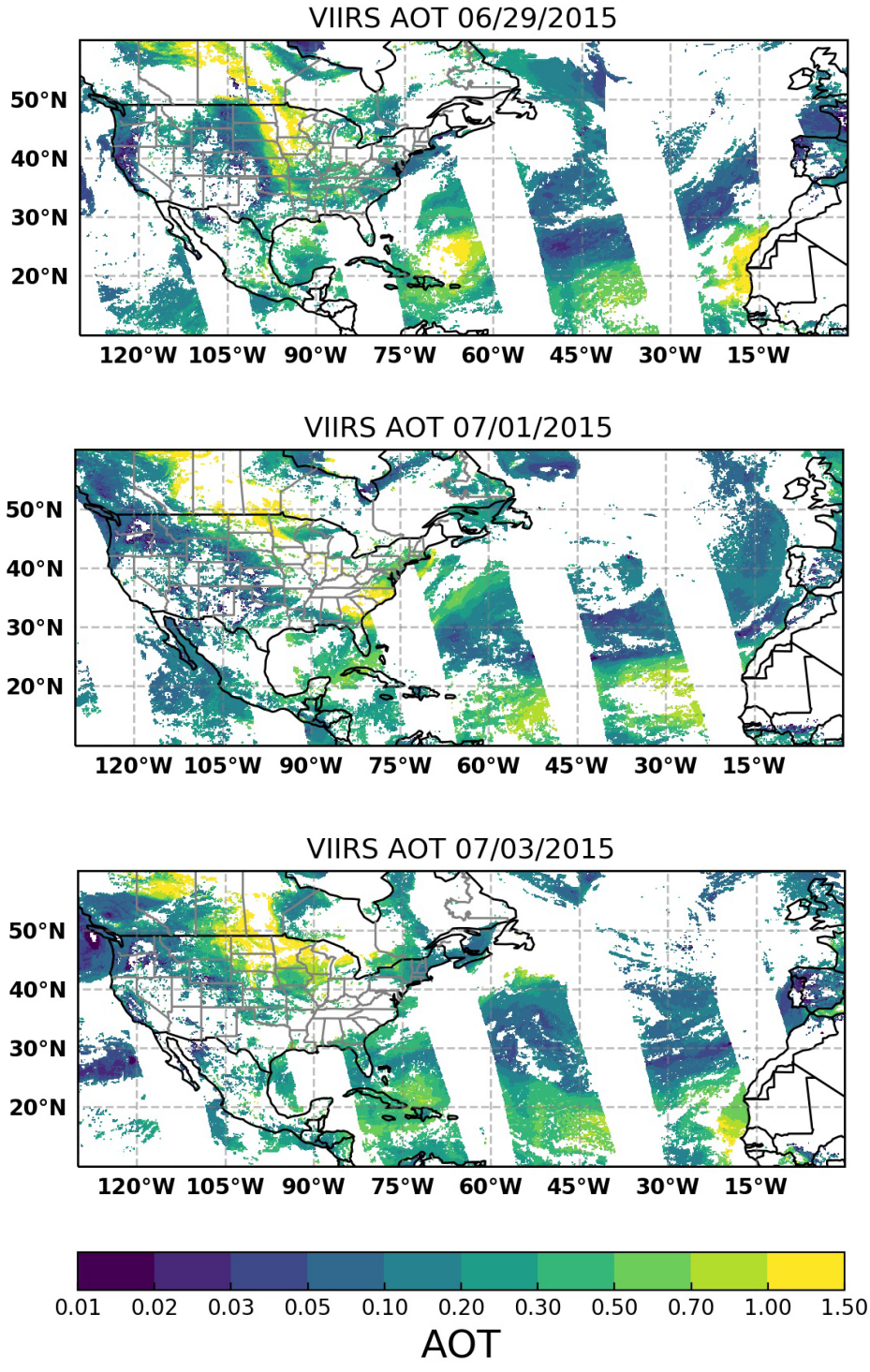

Figure 1. S-NPP VIIRS Aerosol Optical Thickness (AOT) on 06/29, 07/01, and 07/03 of 2015.

https://doi.org/10.5194/acp-2020-587
Preprint. Discussion started: 5 August 2020

Atmospheric Chemistry and Physics Discussions

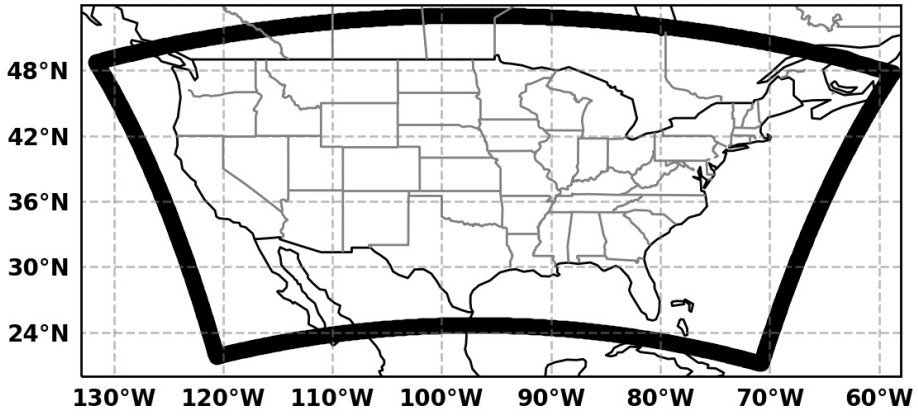

Figure 2, NAQFC CONUS domain (bold black)

https://doi.org/10.5194/acp-2020-587
Preprint. Discussion started: 5 August 2020

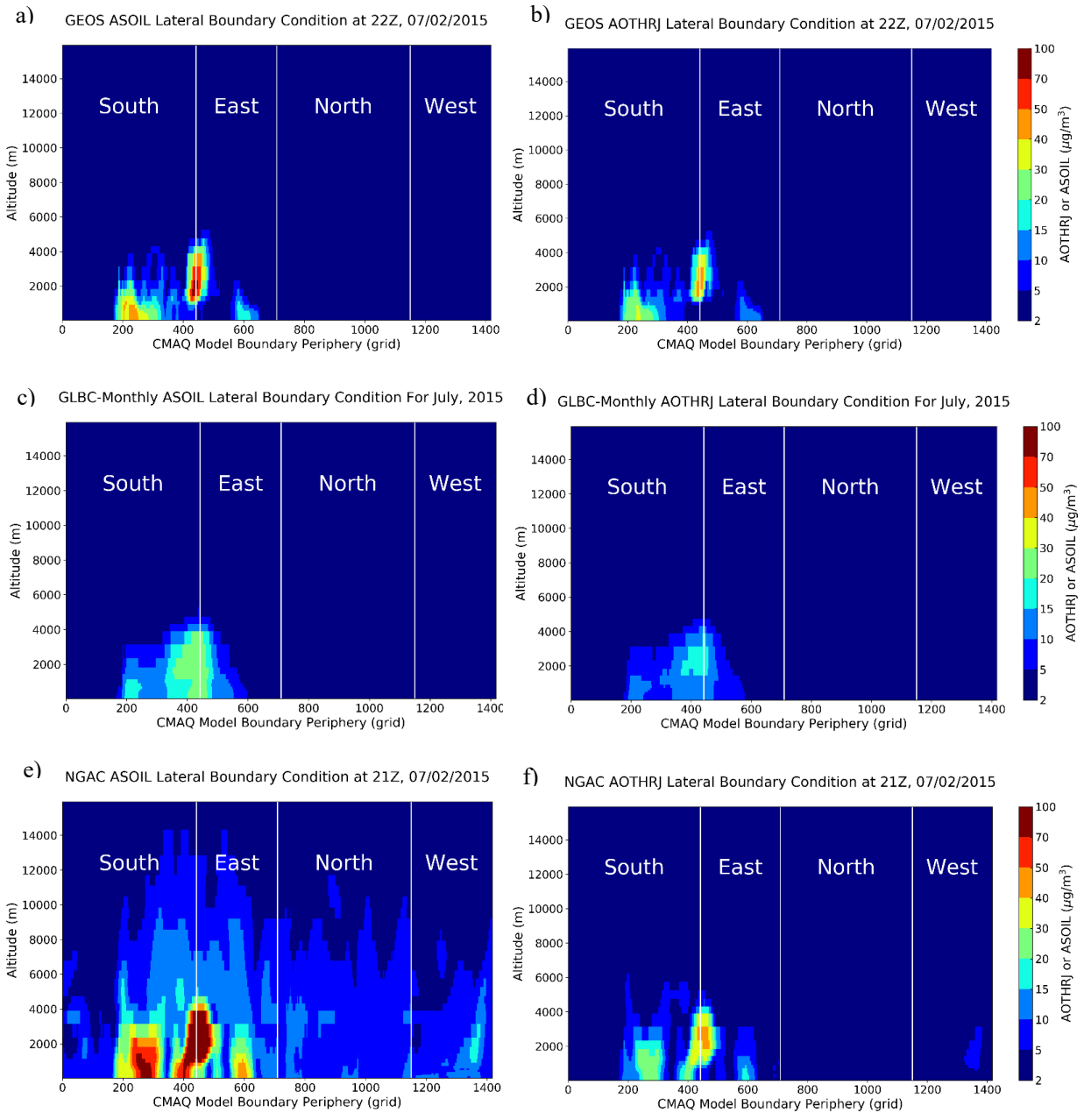

Figure 3. The lateral boundary conditions for ASOIL (left) and AOTHRJ (right) along the domain periphery for July 02, 2015.

https://doi.org/10.5194/acp-2020-587
Preprint. Discussion started: 5 August 2020

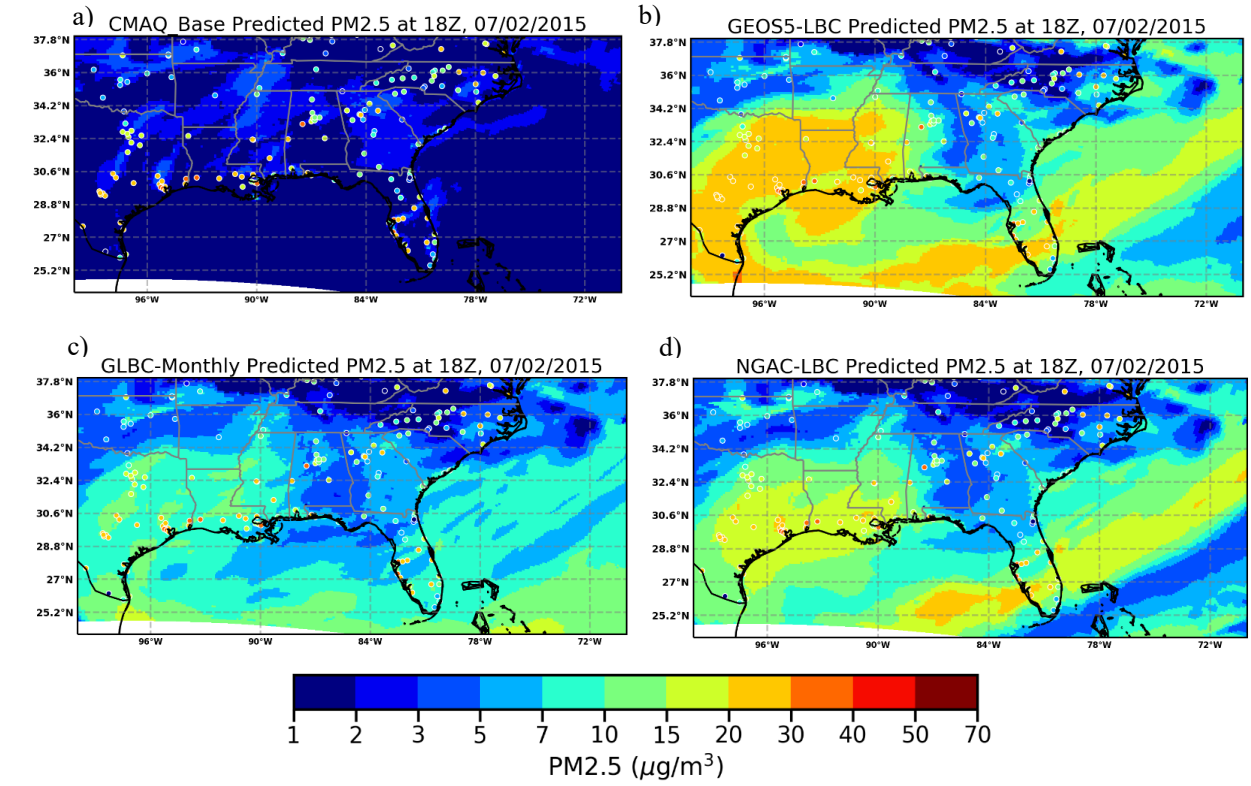

Figure 4. Model Predicted surface PM2.5 with the four LBCs for July 02, 2015 (the colored circles show the AIRNow observations)

https://doi.org/10.5194/acp-2020-587
Preprint. Discussion started: 5 August 2020

Atmospheric Chemistry and Physics Discussions

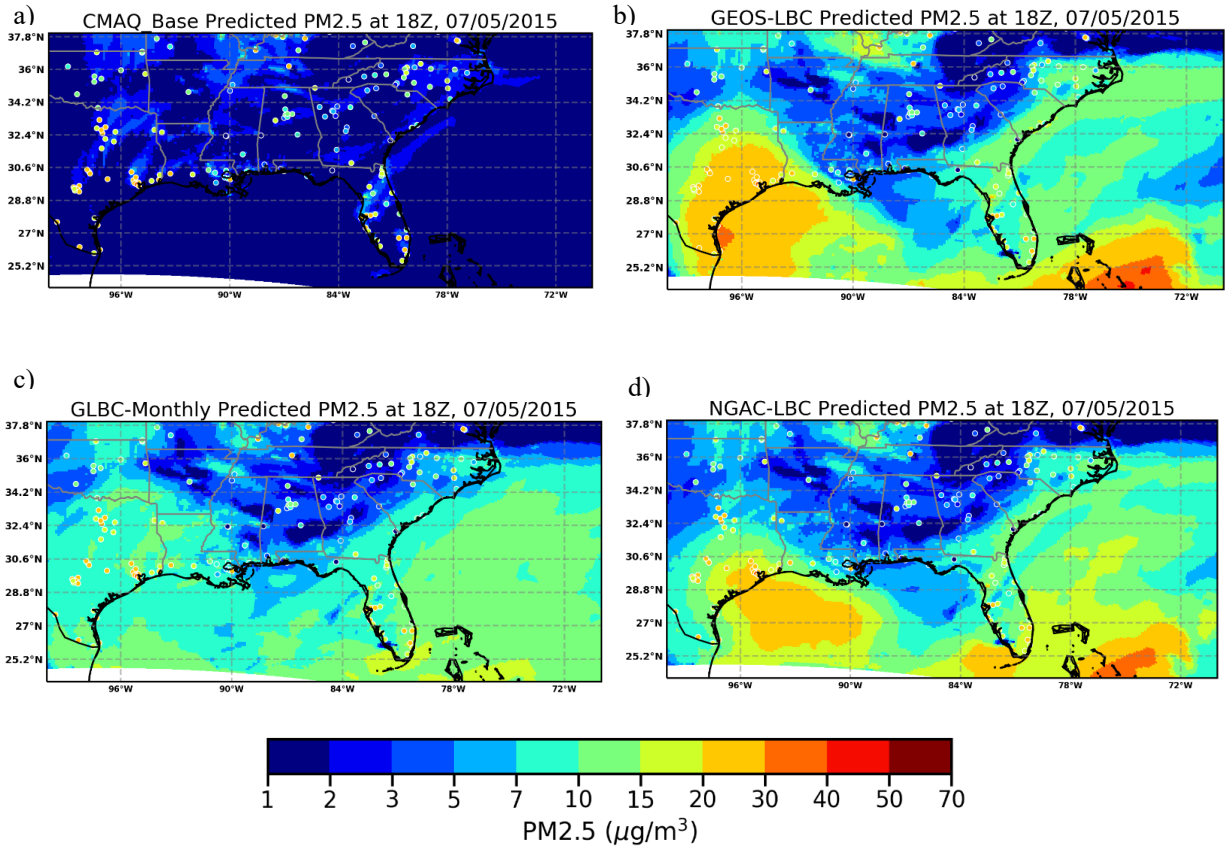

Figure 5. Same as figure 4 but for July 05, 2015

https://doi.org/10.5194/acp-2020-587
Preprint. Discussion started: 5 August 2020

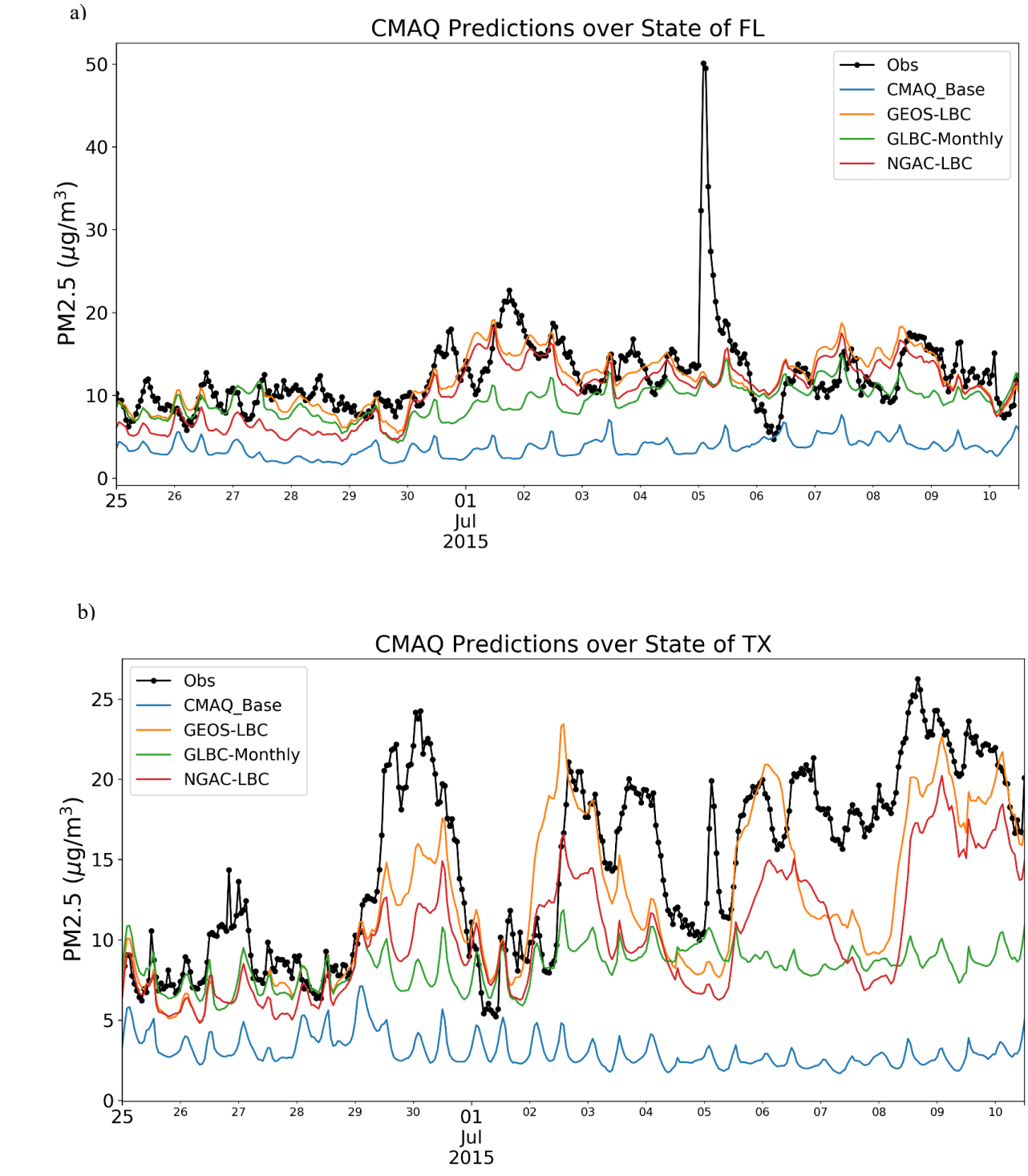

Figure 6. Time-series PM2.5 comparisons over the states of Florida and Texas. All the times are in UTC.

https://doi.org/10.5194/acp-2020-587
Preprint. Discussion started: 5 August 2020

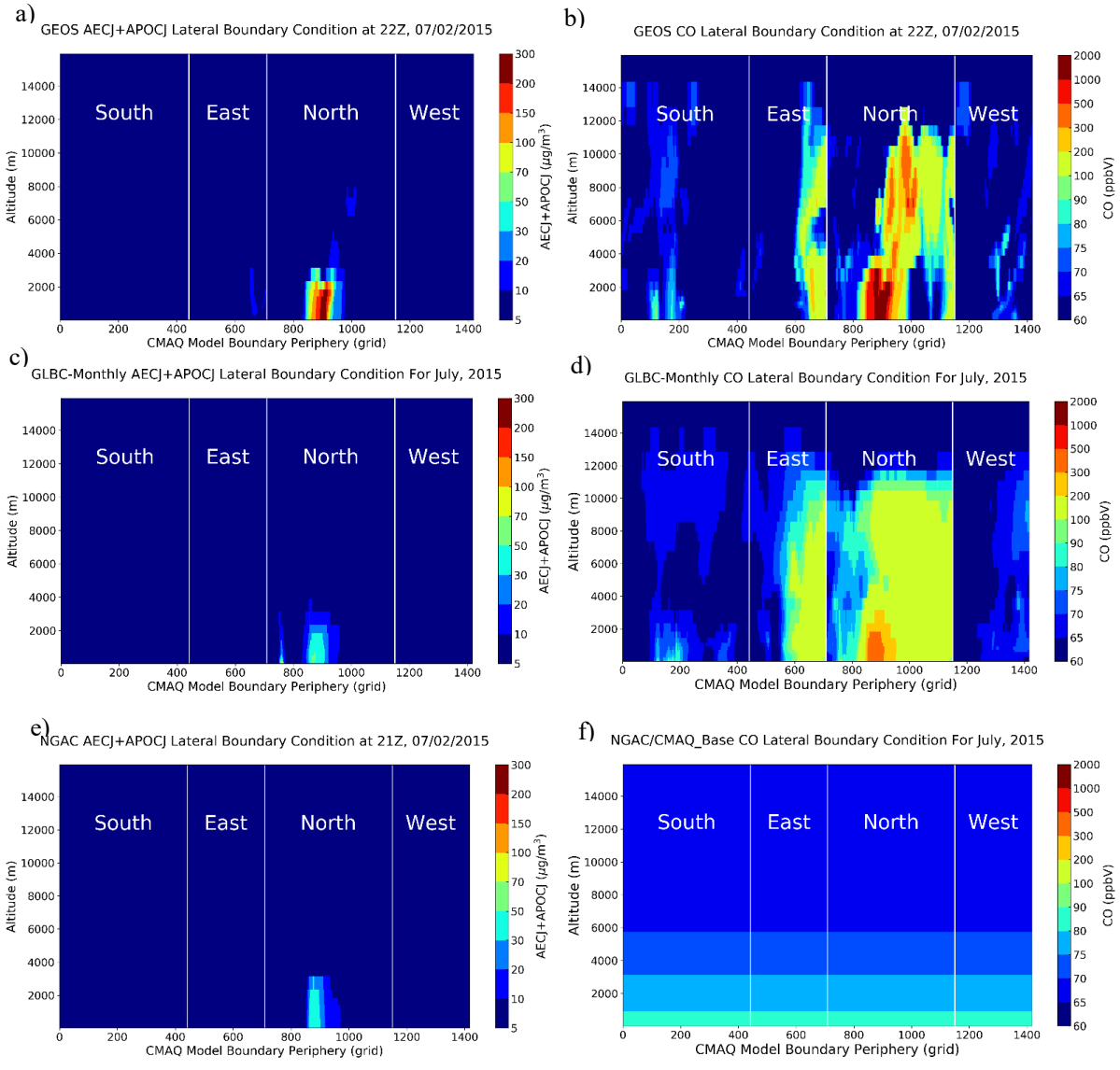

Figure 7, same as Figure 3 except for total EC and POC (AECJ+APOCJ) (left) and CO (right).

https://doi.org/10.5194/acp-2020-587
Preprint. Discussion started: 5 August 2020

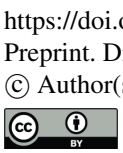

Atmospheric Chemistry and Physics Discussions

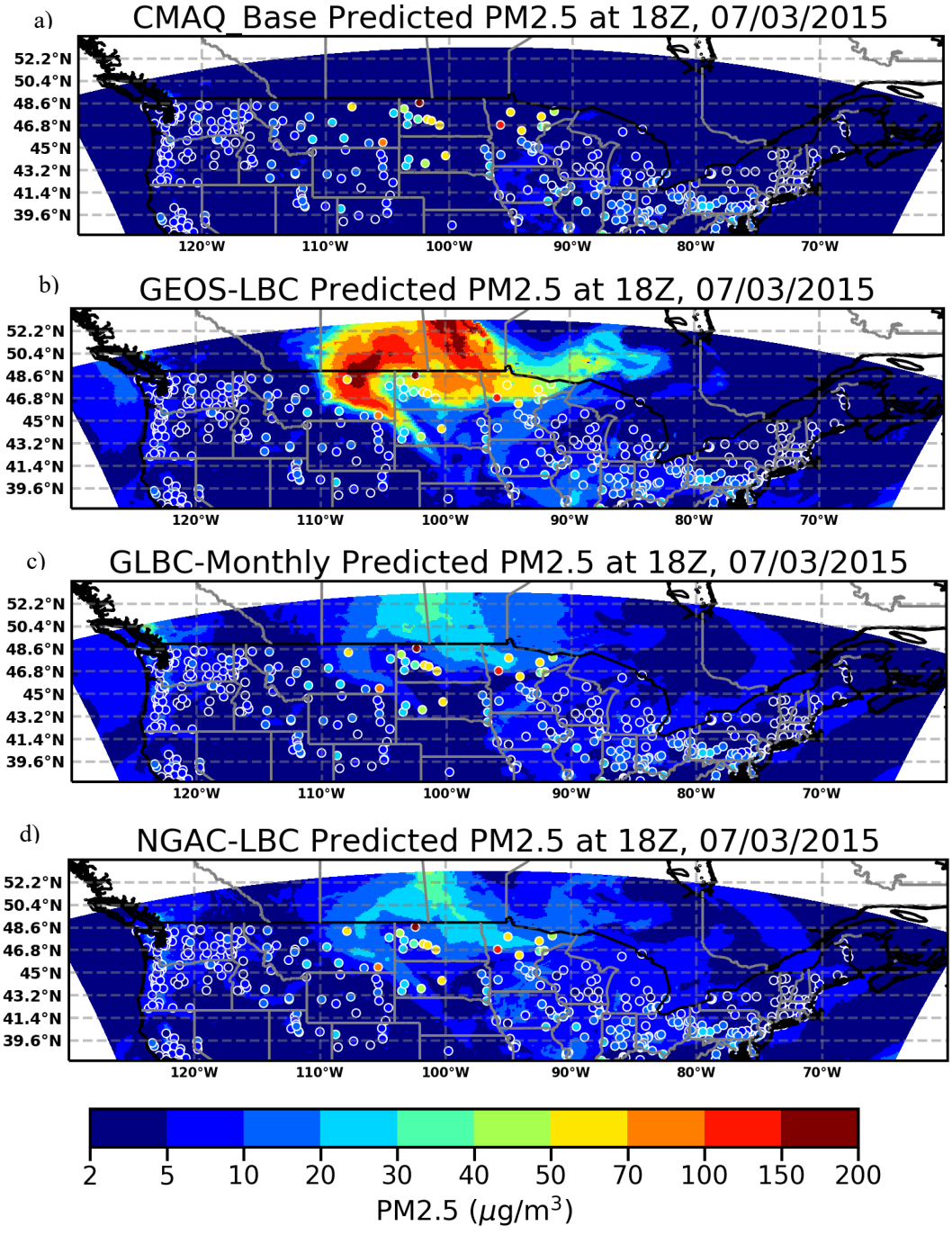

Figure 8, same as Figure 4, but for Northern USA on July 3, 2015

https://doi.org/10.5194/acp-2020-587
Preprint. Discussion started: 5 August 2020

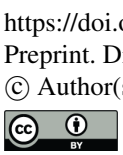

Atmospheric Chemistry and Physics Discussions

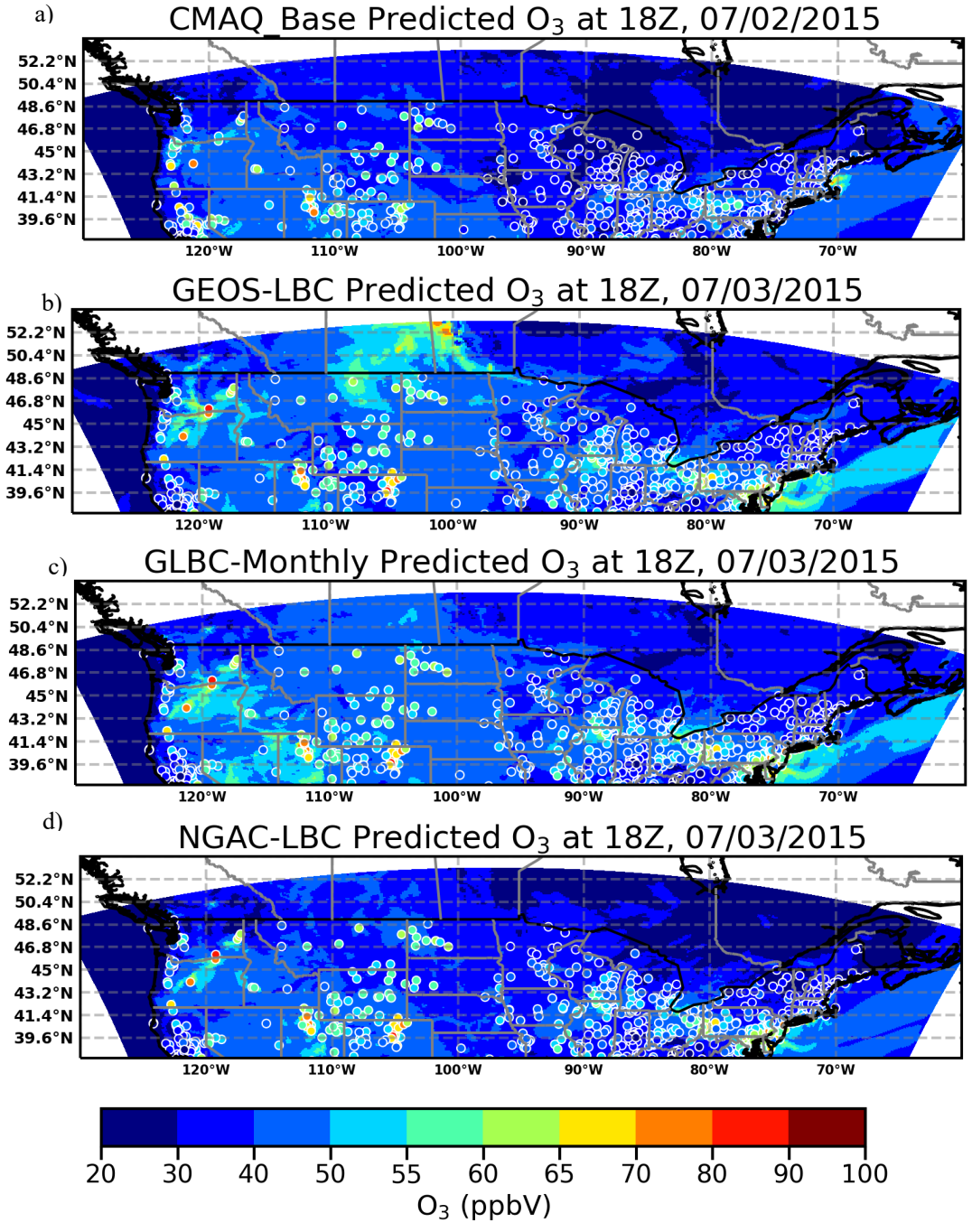

Figure 9, same as Figure 8, but for O_3.

https://doi.org/10.5194/acp-2020-587
Preprint. Discussion started: 5 August 2020

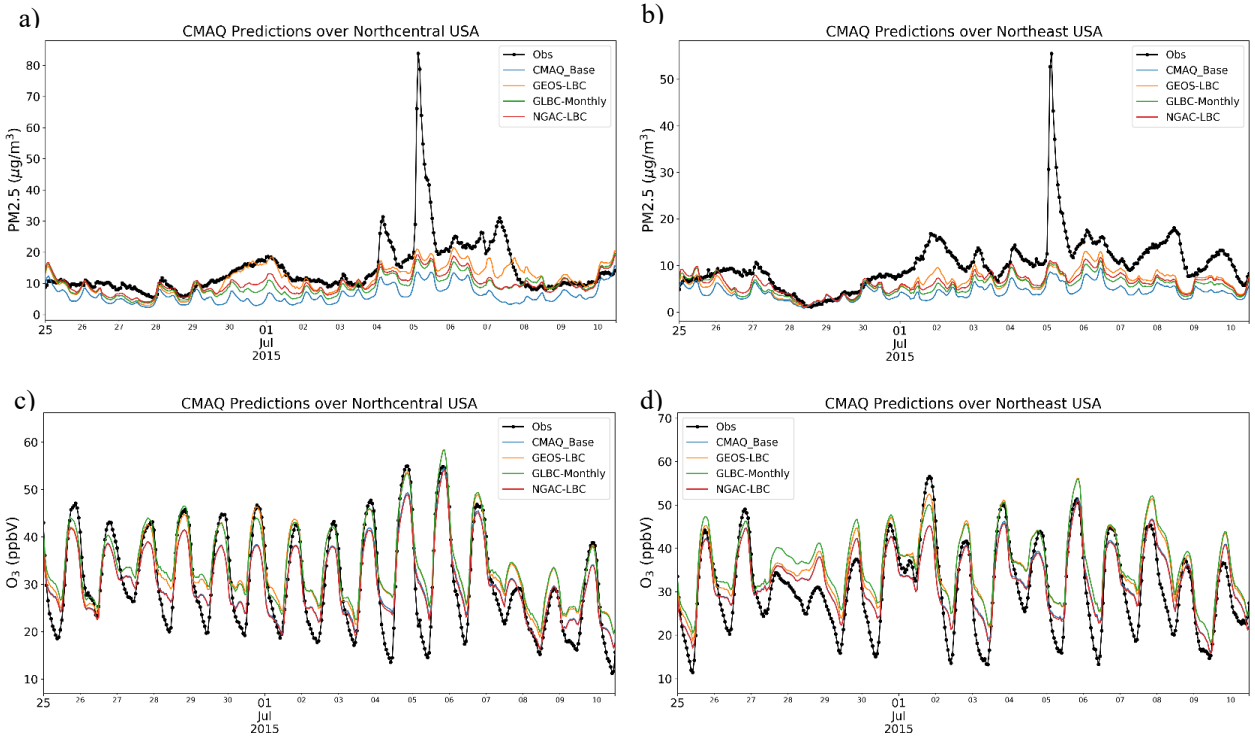

Figure 10. Time-series comparisons for PM2.5 (top) and O_3 (bottom) over the Northcentral (left) (States of Illinois, Indiana, Iowa, Kentucky, Michigan, Minnesota, Missouri, Ohio, and Wisconsin) and Northeastern USA (right) (States of Connecticut, Delaware, Maine, Maryland, Massachusetts, New Hampshire, New Jersey, New York, Pennsylvania, Rode Island and Vermont and District of Columbia). All the times are in UTC.

https://doi.org/10.5194/acp-2020-587
Preprint. Discussion started: 5 August 2020

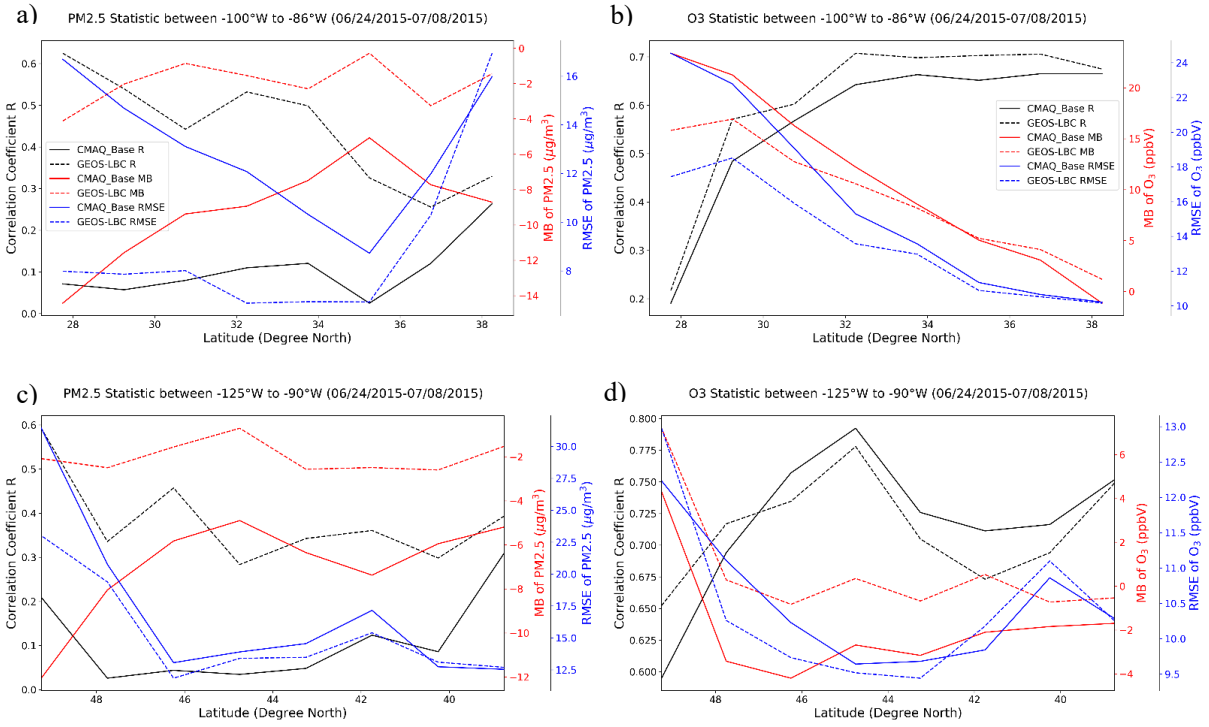

Figure 11, The latitudinal distributions of correlation coefficient R (black), mean bias (MB) (red), and root mean square error (RMSE) (blue) of $PM_{2.5}$ (left) and O_3 (right) from June 24 to July 8, 2015 over Southern USA (top) and Northern USA (bottom) for CMAQ_Base (solid line) and GEOS-LBC (dash line) runs.

https://doi.org/10.5194/acp-2020-587
Preprint. Discussion started: 5 August 2020

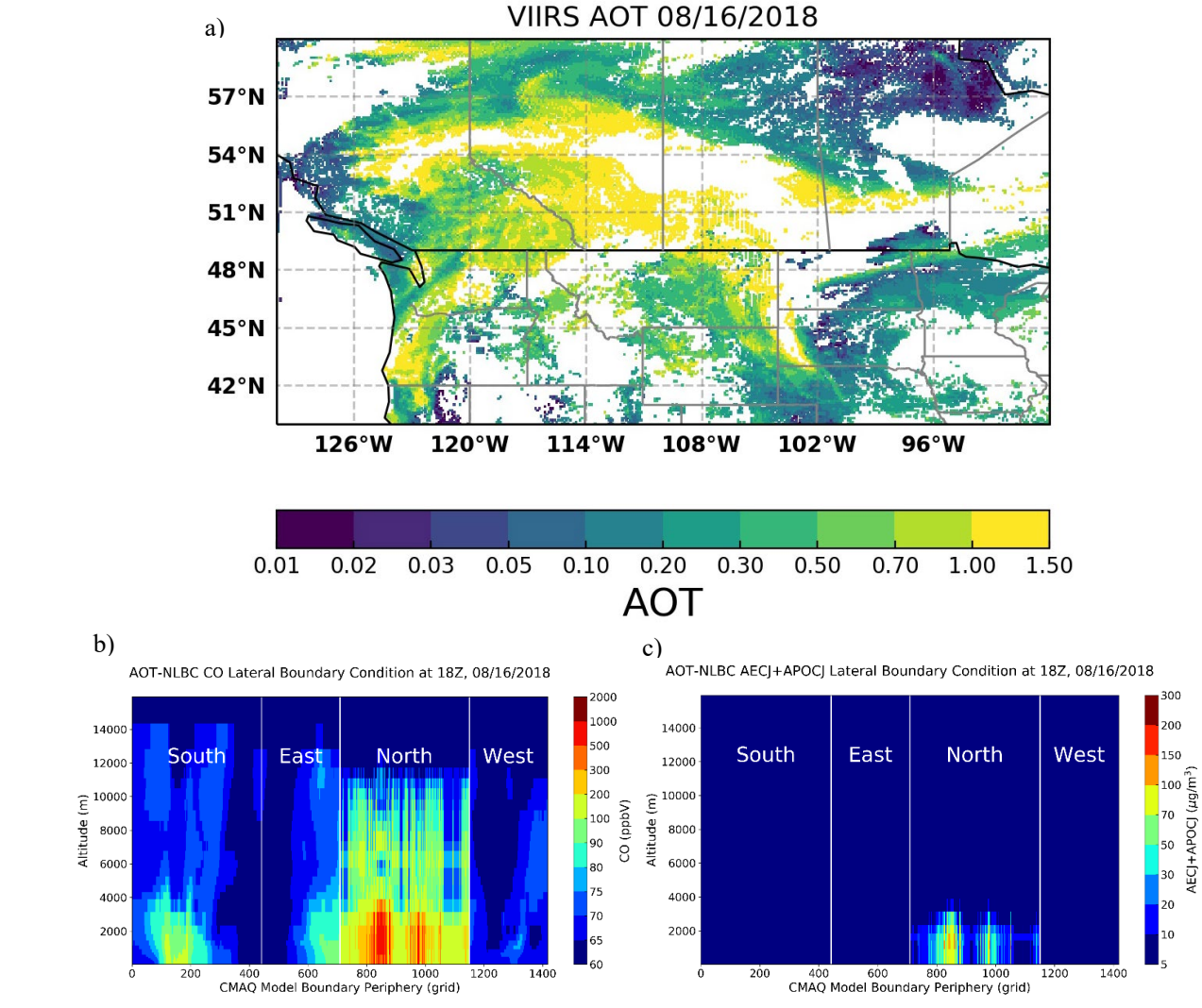

Figure 12. VIIRS-AOT (a) on 08/16/2018 and the corresponding derived AOT-NLBC for CO (b) and AEC+APOCJ (c)

https://doi.org/10.5194/acp-2020-587
Preprint. Discussion started: 5 August 2020

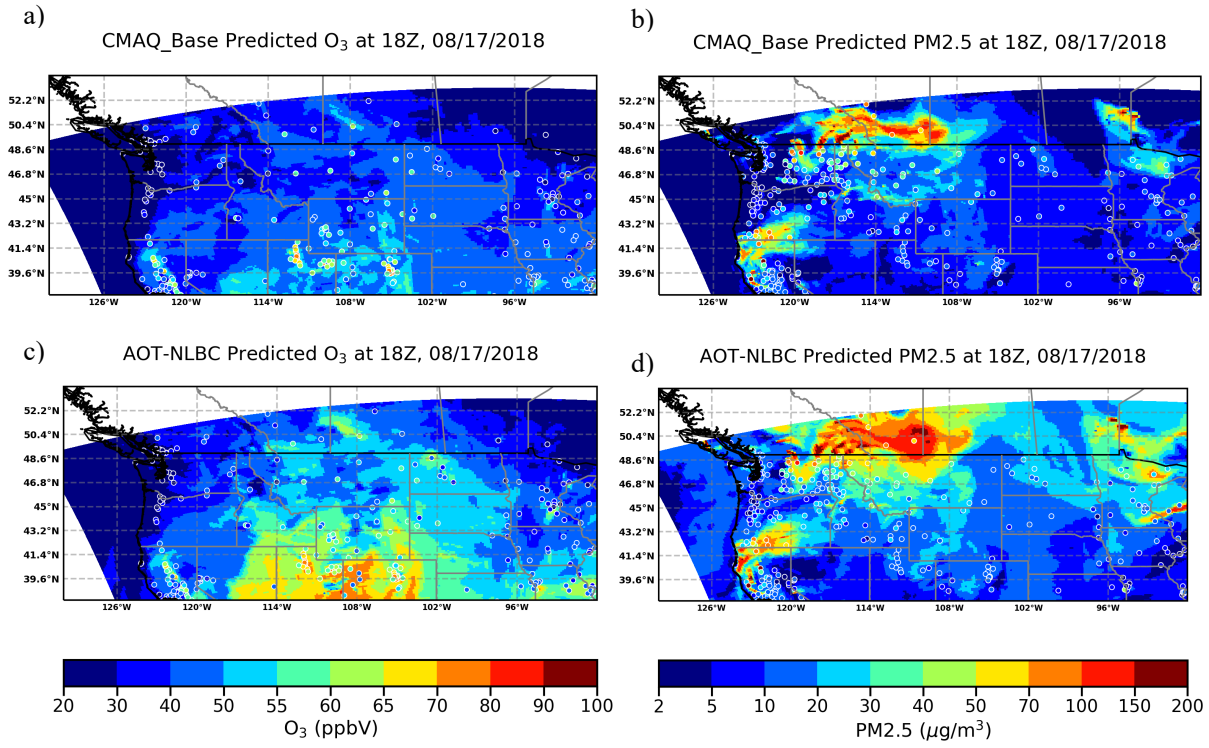

Figure 13. Model Predicted surface ozone (left) and PM2.5 (right) with the CMAQ_Base (top) and AOT-NLBC (bottom) for August 17, 2018 (the colored circles show the AIRNow observations)

https://doi.org/10.5194/acp-2020-587
Preprint. Discussion started: 5 August 2020

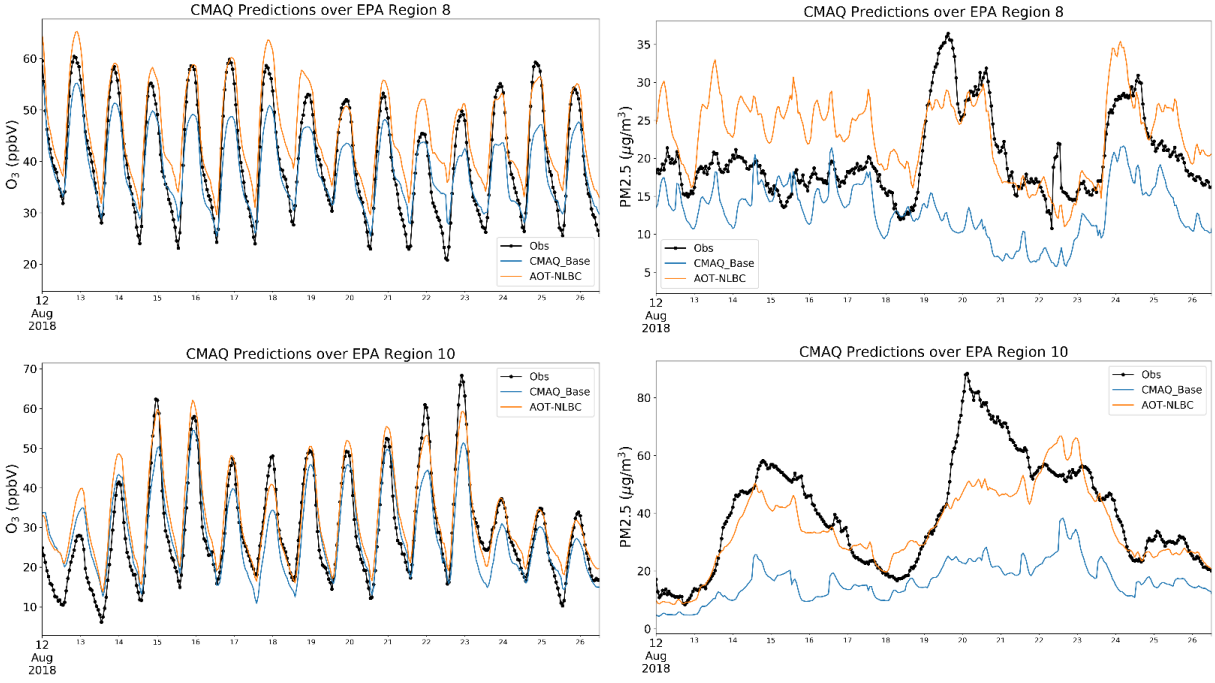

Figure 14, Time-series comparisons for surface ozone (left) and PM2.5(right) over EPA region 8 (states of MT, ND, SD, WY, CO and UT) and region 10 (states of WA, ID and OR) predicted by CMAQ_Base and AOT-NLBC